NACA

RESEARCH MEMORANDUM

INVESTIGATION OF AN IMPULSE AXIAL-FLOW COMPRESSOR

By John R. Erwin and Wallace M. Schulze

Langley Aeronautical Laboratory
Langley Air Force Base, Va.

NATIONAL ADVISORY COMMITTEE
FOR AERONAUTICS

WASHINGTON

February 8, 1950
Declassified April 13, 1953.

NATIONAL ADVISORY COMMITTEE FOR AERONAUTICS

RESEARCH MEMORANDUM

INVESTIGATION OF AN IMPULSE AXIAL-FLOW COMPRESSOR

By John R. Erwin and Wallace M. Schulze

SUMMARY

An investigation was made to determine the possibilities of obtaining high pressure coefficients by applying a constant-pressure high turning principle to impulse axial-flow compressor rotors. In conventional axial-flow compressors, the total pressure coefficient is limited to a maximum of about 1.0 by separation losses that accompany turning angles exceeding about 30°, as a result of the associated static-pressure rise. Turning the flow without static-pressure rise, as in impulse turbines, greatly extends the limit of turning angle, and higher pressure coefficients are possible.

In order to develop blade designs for an impulse axial-flow compressor, blade sections were tested in a 5-inch low-speed cascade tunnel at the Langley Aeronautical Laboratory. From these results, a rotor was designed to produce a turning angle of 75° and a total pressure coefficient of 2.40. This rotor was tested in a low-speed test compressor without inlet guide vanes and with and without stator blades. At the design quantity-flow coefficient of 0.82, a rotor total-pressure coefficient of 2.3 with 98.3 percent efficiency and a stage total pressure coefficient of 2.05 with an efficiency of 89.6 percent were obtained.

INTRODUCTION

The advantages of the axial-flow compressor are in its high specific-flow capacity and high efficiency. The principal disadvantage is the low total-pressure-rise coefficient obtainable with the usual design. This limitation is imposed because the rotor-blade passages are used not only to impart kinetic energy to the flow but also, as diffusers, to convert part of the dynamic pressure to static pressure. This system is desirable when interest is centered largely in obtaining a given static pressure rise with maximum efficiency because, when a constant diffusion efficiency

or constant blade lift to drag ratio is assumed, dividing the static pressure rise equally between rotor and stator has been shown to produce least losses (reference 1). Separation losses accompanying high static-pressure-rise coefficients, however, set a limit to the diffusion and, therefore, to the turning angle. The angle through which the flow is turned is the primary determinant of the amount of energy added to the flow; therefore, with this system, the energy that can efficiently be added to the air is limited.

The flow may be turned through large angles efficiently if little or no static-pressure rise takes place. Such flows exist in impulse turbines. The purpose of the present investigation is to examine the possibility of obtaining significantly greater total-pressure-rise coefficients by using these principles to design an axial-flow compressor rotor. Although conventional compressor turning angles are in the range of 30° and below, impulse turbines normally operate with turning angles of 90° and above, with 120° as a typical value. If this large turning angle could be accomplished efficiently in a compressor, the energy input would be greatly increased. Some prior work has been done in this field. In reference 2, a constant-pressure blower (called the Schicht blower after its inventor) is discussed. Possibilities of such a blower were indicated by the French engineer, Rateau, as early as 1890, but very little attempt was made to develop the idea before the Schicht designs. Reference 2 indicates that, with turning angles of about 45°, efficiencies of over 80 percent were experimentally produced with a pressure-rise coefficient of 0.8 but, with a pressure-rise coefficient of 1.4, the highest efficiency attained was 60 percent. Although the constant-pressure principle was previously established, full advantage of the possibilities was not taken.

In the present investigation the flow was turned more than in the Schicht blower in order to obtain higher pressure coefficients. Another advantage of greater turning was a reduction in the taper of the rotor annulus necessary to maintain constant static pressure. Reducing the taper of the blower passage made the flow more nearly two dimensional and therefore minimized radial flows which complicate the analysis. Axial flows also permitted the direct use of blade sections developed in two-dimensional cascades. It was believed that an efficient high-pressure-coefficient impulse compressor would result when these principles were used. A similar attempt was made by A. Weise (reference 3); however the maximum pressure ratio was 1.4 rather than the value of 2.1 which Weise anticipated. The adiabatic efficiency was very low, of the order of 40 percent. Weise attributed this performance to the observed extremely nonuniform flow leaving the rotor, but he was unable to find a satisfactory explanation for the poor flow.

SYMBOLS

D	diameter, feet
E	power available, foot–pounds per second
I	power input, foot–pounds per second
m	mass rate of flow, slugs per second
n	rotor speed, revolutions per second
p_t	total pressure, pounds per square foot
p_s	static pressure, pounds per square foot
Q	quantity rate of flow, cubic feet per second
q	dynamic pressure, pounds per square foot
r	radius, feet
U	rotational velocity of rotor blade, feet per second
V	velocity of air (relative to casing), feet per second
W	velocity of air (relative to rotor), feet per second
α	angle of attack, degrees
β	stagger angle, degrees
γ	ratio of specific heats of air, 1.4
η	adiabatic efficiency
θ	turning angle, degrees
ρ	air density, slugs per cubic foot
σ	solidity (blade chord expressed as ratio of mean blade gap)
φ	angle of air flow with reference to the rotor axis in stationary coordinates, degrees
ϕ	angle between blade chord line and tangent to mean line, degrees

$\frac{Q}{nD_t^3}$	quantity coefficient
$\frac{\Delta p_s}{1/2\rho U_t^2}$	static-pressure-rise coefficient
$\frac{\Delta p_t}{1/2\rho U_t^2}$	total-pressure-rise coefficient
$\frac{Q}{D^2}$	specific-flow capacity

Subscripts:

a	axial direction
c	entrance chamber
h	hub
i	inboard section
l	local
o	outboard section
R	rotor
S	stage
t	tip
tan	tangential
x	at any point
1	at section entering rotor blades
2	at section leaving rotor blades
3	at section leaving stator blades

AERODYNAMIC DESIGN

General

The purpose of this investigation was to design an impulse axial-flow compressor that would produce a higher total-pressure coefficient than conventional blowers and compressors and yet be of such configuration that the unit could be tested in existing equipment. Nonradial entry into and exit from the rotor were required. As the rotational speeds to be used in practice are expected to be rather low when subsonic stators are employed, a high ratio of axial velocity to rotational velocity was selected (stagger angle $\beta = 45^\circ$) to provide reasonable quantity flows for a given tip diameter. The design quantity flow coefficient is 0.82. Consideration of hypothetical flow-inducing criterions, explained in detail subsequently, suggested a turning angle θ of about 75°.

Two main problems were considered in selecting the velocity diagrams to be established by the compressor. The first problem was that of obtaining a high pressure coefficient. A brief analysis indicated that in the range of stagger angles and turning angles being considered, 45° and 75°, respectively, diffusing the flow in the rotor would reduce the momentum input and, consequently, the total-pressure coefficient, other conditions remaining constant. The ability of the blades to turn the air efficiently while diffusing the flow was also doubtful. With a high static-pressure-rise coefficient in the stator, the development of an efficient stator is a difficult problem. For this reason, a reduction in the static pressure across the rotor was considered undesirable, even though higher total-pressure coefficients would result, because the stator problem would become more difficult for such conditions. An essentially constant static pressure through the rotor was therefore selected. Calculations based on the velocity diagrams for the geometry selected suggest that ideally the design pressure coefficient would be 2.4. The analysis of Perl and Tucker (reference 4) is suggested for the general case.

The second problem concerned the induction of flow through the compressor by the rotor. A turbine normally operates from a separate source of pressure, as a boiler, but a compressor must induce its own flow. Although the flow in turbine and compressor rotors may be aerodynamically similar, care must be exercised in the design of an impulse compressor to insure that steady flow in the desired direction is established by the rotor. Inasmuch as little information concerning the factors which influence the induction of flow into a rotor could be obtained, the velocity diagrams and blade shapes for the inboard station located 25 percent span from

the hub and for the outboard station located 25 percent span from the tip were selected to have some characteristics similar to conventional compressors; thus,

(1) The entrance air direction β_1 would have a larger inclination from the axis than would the exit air direction β_2 (see figs. 1 and 2) with $\beta_1 = 45^\circ$ and $\beta_2 = -30^\circ$ when $\theta = 75^\circ$.

(2) The leading edge of the rotor blades would precede the trailing edge in the direction of rotation.

(3) Vortex distribution of tangential velocity of the flow leaving the rotor would be employed. With a stagger of 45° and a deflection of 75° at the inboard station, without guide vanes a stagger angle of 48.4° results and a deflection angle of 65.9° is required at the outboard station.

(4) An airfoil thickness distribution having a round leading edge and a sharp trailing edge would be used.

(5) A hub-to-tip radius ratio of 0.78 at the inlet to rotor would be used.

Blade sections were desired which would have the highest critical Mach number obtainable for the condition of constant velocity through the rotor. Blade sections having circular-arc mean lines which closely approximate this condition were selected.

The impulse rotor blades are required to turn the flow through angles significantly greater than the angles used in conventional compressor blades. For this reason, blade solidities of about 2.0, approximately equal to those of impulse turbines, were employed.

A configuration with the leading edge forward of the trailing edge was desired. An estimate based on turbine-blade design experience indicated that, with the use of circular-arc mean lines and a blade solidity $\sigma = 2.0$, the camber angle of the mean line would be 15° greater than the desired turning angle of 75°. Under these conditions, with 45° stagger the tangent to the mean line at the leading edge is 50° from the axial direction, and the tangent at the trailing edge is -40° from the axial direction. With a circular-arc mean line, then, the leading edge precedes the trailing edge. (See fig. 3.)

If these flow angles are used, a contraction of passage area is required to obtain equal static pressures upstream and downstream of the rotor. Inasmuch as a change of tangential velocity occurs in the rotor, a spanwise static pressure gradient is required for nonradial flow. The static pressure can thus be constant in the axial direction at only one radius. In order to avoid static-pressure decrease at any radius, this condition must exist at the inner casing. Because of the fairing inserted on the inner casing and the expected boundary layer, the constant-pressure condition was designed to occur at a position 25 percent of the blade span from the hub.

Although the impulse-compressor stage tested was intended to simulate a unit from a multistage compressor, a condition of no prerotation of the flow entering the rotor was selected because of the difficulty of accurate measurement downstream of stationary blade rows. The losses of such a guide vane row are believed to be low and detract little from the performance.

Experimental Development of Rotor Blade Sections

The turning angles required of the blade sections for the impulse compressor were well beyond those used in conventional compressors. For this reason, a blade design based on results of turbine blade tests was selected. For the solidity used and the turning angle selected a mean-line camber angle $(\phi_1 + \phi_2)$ of 90° was estimated to be necessary. A few cascade tests in which the apparatus described in reference 5 was used were run to provide a check on this estimate and to insure that satisfactory blade-surface pressure distributions were obtained. At the time of these tests, cascade testing techniques at Langley were in an early stage of development and the results are to be considered of a qualitative nature only.

The design conditions $\beta = 45°$ and $\theta = 75°$ for the inboard section of the rotor blade, located at 25 percent span from the inner casing, were quite similar to typical impulse-turbine blade conditions. A turbine blade section was thus believed satisfactory for this purpose. Accordingly, a turbine section was tested in a 5-inch low-speed cascade tunnel at Langley. The section maintained an approximately constant flow-passage area when used in conjunction with a reduction in blade span introduced in the rearward half of the passage. This section was tested with and without a fairing piece on one wall of the tunnel to provide the reduction in span. The fairing varied linearly in thickness from zero at midchord to 0.68 inch at the trailing edge of the blades. The results of these tests and a sketch of the blade (blade 1) are presented

in figure 4. The very high values of q_2/q_1 recorded were undoubtedly due to the rather large thickness. High values of q_2/q_1 are indicative of low critical blade Mach numbers and limit the entrance velocities and the power input to the flow. The desired turning angle was obtained when the fairing was inserted and thus the solidity and camber estimations were verified.

With these two points in mind, a circular-arc airfoil having an NACA 65-010 thickness distribution (blade 2, fig. 5) was constructed. Following previous airfoil practice, the thickness was distributed in percent of the chord. With this highly cambered mean line, however, a section having very thin leading and trailing regions resulted. When tested in cascade, this section proved to be very sensitive to angle-of-attack changes and was considered impractical. The blade and its pressure distribution, with and without the 0.68-inch fairing piece, are presented in figure 5. Without the fairing, a turning angle of 74° (about 1° lower than the desired value indicated) was measured. With the fairing installed, the desired turning angle was obtained.

The next step was to lay out a blade having the NACA 65-010 thickness distributed in proportion to the mean-line length. A somewhat more reasonable airfoil resulted. With a mean-line camber angle of 90°, a turning angle of 74° was obtained with constant span. With the fairing installed, a turning angle of 75° was measured. The pressure distributions and a drawing of the blade (blade 3) are given in figure 6. Because of higher values of q_2/q_1 in the forward region, this section is not considered to be the best that could be evolved. Inasmuch as the purpose of this low-speed investigation was primarily to determine whether such a compressor would operate, no further improvement of this section was attempted.

Selecting the constant static-pressure condition at the inboard section requires the outboard section to produce a static-pressure rise. Vortex distribution of tangential exit velocity from the rotor prescribes the vector diagram for the outboard station, once the inboard velocity diagram has been determined. With the outboard section located 25 percent span from the outer casing, a turning angle of 65° from the entering stagger ($\beta = 48.5°$) is required. The empirical methods used in designing the inboard section were again employed. In order to obtain blades having similar sections at all radii, a circular-arc mean line with NACA 65-010 thickness distribution was used at this station. The complete blade was obtained from the sections at the inboard and outboard stations by straight-line generatrix.

This section was tested with and without the fairing used in the previous tests. This procedure was necessary because all sections in the rotor are believed to be similarly affected by a change of flow area, whether the change is accomplished by altering either the inner or the outer casing.

The desired turning angle was achieved in the first attempt, but again the observed pressure distribution indicated that an optimum section for high-speed operation was not obtained (fig. 7). A smaller increment of local and exit velocities was noted when the fairing was installed. This result was perhaps due to thicker boundary layers in this pressure-rise case. With the fairing in, a lower pressure rise and thinner boundary layers resulted, and the geometrical reduction in passage exit area was thus masked.

The significant dimensions of the rotor blades are presented in figure 8. A photograph of a typical blade is presented in figure 9.

Stator Design

Inasmuch as the impulse rotor by definition does not increase the static pressures, this burden falls on the stator blades. When satisfactory rotor blades had been obtained, therefore, it was necessary to test a rotor-stator combination in attempting to evaluate the possible performance of impulse compressors. The stator configuration investigated was one which discharged the flow with an exit tangential velocity similar to that of an intermediate stage of a multistage compressor.

The stator was designed after the rotor had been tested. From the rotor-alone tests, the exit flow at design quantity coefficient (0.82) was known. The stator was designed to turn this flow about 21° with a vortex distribution of tangential velocity at the stator exit. Ideally, stator blades having a small camber variation would have been required if each section were to operate at its design point. For reasons of simplicity, a blade having sections of constant camber was used. From the charts of reference 5, NACA 65-(12)10 sections were selected for the three design diameters. (See fig. 10 for sketch and coordinates.) This simplification probably reduced the high efficiency range but should have had little or no effect on peak efficiency, since all sections operate near their design points at design quantity coefficient.

APPARATUS AND METHODS

The 75-horsepower low-speed test compressor used in this investigation (described in reference 6) was modified to the configuration shown in figure 11. For these tests, a radial diffuser was added at the exit of the axial diffuser. A spoiler-type throttle was attached to the exit of the radial diffuser.

The outer casing had a diameter of 27.82 inches. The hub diameter of the rotor was 21.82 inches. The hub-to-tip radius ratio of 0.78 represents an average condition in typical compressor application. Beginning midway through the rotor blades, balsa fairings were glued to the hub and the diameter increased linearly to 23.0 inches at the trailing edge of the blades. For one series of tests (A series) this diameter was held constant to a point 2 inches downstream from the stator. For a second series (B series) this constant diameter was extended 24 inches beyond the stator to a point downstream of station 3'. The existing rotor hub had provision for 26 blades. A chord of 5.5 inches was used to obtain a chord-gap ratio of 2. The tip clearance varied from 0.008 inch to 0.015 inch, or less than 1/2 percent of blade span.

The annular height was maintained constant from the rotor blade exit to a position downstream of the stator exit. Twenty-seven stator blades of 4.5-inch chord and solidity of 1.5 were used. Flow-survey instruments were located forward and rearward of the rotor and in a ring, which could be rotated, downstream of the stator.

Instrumentation

The survey instruments were mounted in suitable relative positions at the several stations so that the wake of one would not affect the flow near a following instrument. All instruments, therefore, could be in place while readings were being taken, and all measurements could be made simultaneously.

A conventional null-method claw-type yaw meter having total- and static-pressure tubes located as shown in figure 12, instrument I, was first used at stations 1, 2, and 3. (See fig. 11.) The measured values from stations 1 and 2 appeared to be reliable in every case, but difficulty was encountered with station 3. In the first series of tests, this survey was made 1.8 inches, approximately 1/2 chord in the direction of the chord, behind the stators where the wakes were quite severe. The pressure and

direction values of the flow had large gradients in the wakes (figs. 13 and 14) and no instrument was available that would accurately survey such a flow field. Instrument II, a conventional pitot-static tube with short yaw tubes downstream of the static orifices (fig. 12), was designed in an attempt to take readings in the stator flow fields and was used at station 3 for the A series of tests. This instrument exhibited high yaw sensitivity but was not ideal for the severe flow conditions present because null readings could be obtained at more than one angular position. The null angles were widely separated and, therefore, the final data are reasonably accurate as is shown hereinafter. The results of these tests are believed to be reliable to within 1 or 2 percent.

The third instrument was an attempt to overcome the undesirable characteristics of instrument II. All readings were taken from a small, undivided part of the flow. The total-pressure tube was conventional except for location but the static-pressure values were taken from the yaw-tube readings. These yaw tubes were carefully filed to the angle that would indicate true static pressure when nulled for yaw reading. This condition was obtained by trial-and-error procedure in the compressor. Comparison was made with a small standard static-pressure probe located at the same diameter in the same axial plane but 30° away. The instrument was used in the B series at a distance of 5 chords behind the stators so that accurate data could be obtained with fewer test points. All static-pressure readings of instruments were calibrated to an accuracy of ±0.2 percent of the dynamic pressure. The direction readings were accurate to ±1/4°.

Operating Procedure

In operation of the impulse compressor, as with more conventional designs, some difficulty was experienced in establishing low quantity-coefficient flows. The throttle had to be opened momentarily to a higher flow condition to unstall the compressor. For such runs, this starting operation was begun at low rotational speed; then the speed was increased to the usual test value of 1200 rpm. The test range was covered by runs made at seven equally spaced values of quantity coefficient from open throttle to surge and several check runs near the design value of 0.82.

Two series of tests were made. In series A, flow measurements were taken at stations 1, 2, and 3, as indicated in figure 11. At stations 1 and 2, surveys were made along one radial line at 15 to 21 radial positions. At station 3, with instrument II downstream of the stator, 12 to 15 survey points were taken along 12 to 19 radial lines covering two stator passages. These surveys were later

averaged by mechanical integration. Care was taken to restrict the integration to the flow field of one blade passage.

In series B tests, surveys were taken at stations 1 and 2, as before, but the surveys made downstream of the stator were taken at station 3'. At station 3', measurements consisted of 12 survey points along each of four radial lines spaced 90° apart. Instrument III was used. Each radial survey was mechanically integrated as before. The four integrations from station 3' were arithmetically averaged.

As these surveys were being made, frequent temperature readings were made of the manometer alcohol and of the air for both dry and wet bulbs. The barometric pressure and time of test were also recorded. The entrance chamber static pressure was taken every time a survey instrument was read and was used as the reference base pressure for all calculations. The value was very nearly equal to atmospheric pressure.

RESULTS AND DISCUSSION

Rotor Alone

In the first series of tests with the impulse compressor, only the rotor was installed in the test setup. The addition of a radial diffuser to the exit of the axial diffuser was necessary to obtain flow through the compressor. This need for a radial diffuser was evidently due to the lack of a static-pressure rise produced by the rotor and to the fact that most of the energy input to the flow appears as tangential velocity. With the radial diffuser, the rotor performance was very satisfactory, A wide operating range with mild stall characteristics was observed. In general, the rotor-alone behavior was quite similar to that of conventional low-speed axial-flow compressors (reference 6).

The flow upstream of the rotor was quite uniform and exhibited only a thin boundary layer and only ±1° of deviation from the axial direction. Typical cross-channel plots obtained by surveying along one radial line downstream of the rotor (station 2) are presented in figures 15 and 16. The total- and static-pressure curves indicate the type of variation from design normally observed in investigations such as this. The measured turning angles presented are not corrected for the higher exit axial velocity (than design) and appear to be low by 3° to $3\frac{1}{2}$° in the center of the annulus. Consideration of figure 17, however, indicates that turning angles corrected by the

method presented in conjunction with figure 42 of reference 5 would yield design values because the tangential velocities are very close to those as estimated, whereas the axial velocities are high in the center of the annulus. No allowance for boundary layers was made in selecting the annular area at the exit of the rotor; therefore, somewhat higher axial velocities might have been expected.

Design velocity diagrams for the inboard section $\frac{D_i}{D_t} = 0.839$, diameter of 23.32 inches, and for the outboard section $\frac{D_o}{D_t} = 0.946$, diameter of 26.32 inches, are presented in figure 1. Experimental values (fig. 2) indicate that a close approach to the design conditions was reached, although slightly high exit axial velocities were measured, as previously indicated.

Estimated rotor-performance curves, based on the cascade test results, are presented in figures 18 and 19. The measured total-pressure-coefficient plot (fig. 18) exhibits the same trends as the calculated curve, but with values about 8 percent lower. Rotor static-pressure coefficients were almost equal with estimated values (fig. 19). The predicted turning angles (fig. 20) are based on cascade tests at fixed stagger angles. As the rotor stagger angle increased with increasing angle of attack, divergences of the type observed at angles of attack above and below design are not unexpected. At low staggers, a steeper slope of θ against α was measured, whereas at higher staggers a lower slope was measured than was obtained in cascade. Acceptable agreement with estimated performance is believed to have been achieved.

Very high efficiencies (about 98 percent) were obtained (fig. 21) with a total-pressure coefficient of 2.3 at design quantity coefficient of 0.82. Efficiency values presented have been corrected by the methods outlined in the appendix. A performance characteristic different from conventional axial-flow compressors is the increasing total pressure with increasing quantity coefficient (fig. 18). The stability of operation was excellent at all quantity flows above stall.

Rotor and Stator

A series of tests of an impulse compressor stage were made to obtain information concerning operating performance and characteristics. The operating characteristics did not significantly change with the addition of the stators. Typical total-pressure, static-pressure, and averaged exit-flow-direction results obtained by surveying downstream of the stator are presented in figures 13, 14, and 22. A peak efficiency of 89.6 percent was obtained at design quantity flow (fig. 21). This peak stage-efficiency value is only a little less than, or is equal to, efficiencies obtainable with conventional axial-flow compressors. This comparison is not strictly exact, because the discharge from the stator was not axial as would be the case for a single-stage blower, nor was there prerotation in the inlet to the rotor as would be the case for an intermediate stage of a multistage compressor. A gradual decline in efficiency was observed at higher or lower flows than the design flow. The stage static-pressure coefficients (fig. 18) are appreciably below values estimated from cascade results. The calculated values assumed no losses, however. In order to determine whether the discrepancy was due mainly to the rotor or to the stator, figure 19 was prepared. As the rotor static-pressure coefficients approach design values, most of the discrepancy is seen to be chargeable to the stators. Consideration of the stator performance in detail indicates that, since the rotor total-pressure coefficient is less than the design value, less energy is available to the stators than calculations indicate. A third of the difference noted can be attributed to this factor (fig. 19). If the measured stator turning angles were below the design angles, a lower static-pressure rise would be expected. Figure 23, however, illustrates that the average turning angle is perhaps a degree greater than estimated. The discrepancies between calculated and measured stator static-pressure rise, therefore, are assumed to be due to flow losses. The stage total-pressure coefficient (fig. 18) indicates a slight increase with increasing flow quantity similar to rotor-alone results. A total-pressure coefficient of 2.05 was measured at design conditions.

An attempt was made to obtain more reliable data by surveying the flow from the stator blades 22.5 inches downstream of the stator (station 3'). At this location, the wake gradients were much less severe than at station 3. The mass flow measured at station 3' agreed with that measured at station 2 within ±2 percent; whereas that measured at station 3 differed by as much as 5 percent. (See appendix.) The stage efficiencies obtained from the readings at station 3' were appreciably lower than that at station 3 and varied from −3.4 percent at low flows to −9 percent at the highest flow. The differences are believed to be due to the inefficiency of the annular diffuser having large inflow angle. Reference 7

indicates that for inflow angles in the range of this investigation (30°), an 8° diffuser would have an efficiency of from 50 to 70 percent. As the kinetic energy entering the diffuser increases with increasing flow quantity for this installation, the over-all efficiencies would be expected to be lower at station 3' than at station 3 by some direct function of quantity coefficient. In general, the results obtained at station 3' indicate the same rotor-stator efficiency trends as obtained from the surveys of station 3.

A method of improving axial-flow-compressor efficiency has been suggested in the use of boundary-layer control. Presumably, this improvement could be accomplished with stationary blades and casings more easily than with rotating members. Inasmuch as the rotor efficiencies measured were very high, perhaps the impulse compressor offers a means of obtaining high efficiencies as well as high pressure coefficients.

EXTRAPOLATION OF LOW-SPEED TEST RESULTS TO HIGH SPEEDS

In order to estimate the pressure ratio per stage obtainable if the test impulse compressor were operated at higher speeds, calculations were made by using performance values measured at low speed. From low-speed cascade results, the allowable operating Mach number of the rotor blades was obtained. When the Kármán-Tsien extrapolation and the maximum value of q_2/q_1 observed, 1.64, are used, sonic velocity would be expected when an entrance Mach number of 0.66 was reached. Preliminary information indicates that high losses do not occur until local Mach numbers are somewhat above 1. (See reference 8.) The impulse-rotor design presented herein should operate efficiently with an entrance Mach number of 0.60. Further blade improvement should make possible the use of somewhat higher values.

For the first extrapolation, the vector diagram used was the same as that shown in figure 1, but the values were increased so that a Mach number relative to the rotor blades of 0.60 would be obtained at the mean diameter. This condition would be reached with a mean rotational speed of 481.5 feet per second and a tip speed of 540 feet per second if the test hub-to-tip ratio of 0.78 were employed. The axial velocity would be 450 feet per second, somewhat less than the maximum used in conventional compressors. The stator Mach number for this case is 0.80. At the turning angle required of the stators, blade sections having critical Mach numbers as high as 0.80 are entirely feasible. Thus the stator does not limit the operating Mach number selection made from consideration of the rotor. Using

the rotor and stage efficiencies obtained in tests yielded a static pressure ratio of 1.37 per stage. This value is higher than values obtained in any production axial-flow compressor, even though usual tip speeds are in the range of 1000 to 1100 feet per second.

A second calculation is presented for a design employing 60° of prerotation in the direction of rotation upstream of the rotor (fig. 24). Prerotation permits higher rotational speed without exceeding a rotor Mach number of 0.60. Although the entrance axial velocity would be 430 feet per second, low hub-to-tip ratios would permit specific flows that approach those of supersonic compressors. Supersonic velocities into the stator blades result. At a rotational speed of 1205 feet per second, a total-pressure ratio of 2.14 per stage would result if the efficiencies measured at low speed are assumed. Although this is not conservative, no great error is believed to be involved, as the stator Mach number is quite low (M = 1.42). At this value, the total-pressure recovery of a normal shock is 95.3 percent. Using these assumptions resulted in curves of total pressure ratio, stator Mach number, and blade rotational velocities for guide-vane turning angles from 0° to 60° (fig. 25).

Because of the high-pressure ratios obtainable at relatively low rotational speeds, impulse compressors offer advantages in various fields.

CONCLUSIONS

An investigation to determine the possibilities of obtaining high pressure coefficients by applying a constant-pressure high turning principle to impulse axial-flow compressor rotors indicated the following conclusions:

1. An impulse compressor rotor, which turns the air 75° from an entering stagger angle of 45°, has been designed. In low-speed tests, this rotor produced a total-pressure coefficient of 2.3 at a static-pressure coefficient of 0.2 with an efficiency of 98.3 percent at a design flow coefficient of 0.82.

2. An impulse compressor stage, consisting of the aforementioned rotor and a conventional stator, produced a total-pressure-rise coefficient of 2.05 with an efficiency of 89.6 percent at design quantity-flow coefficient.

3. The operating behavior of a single-stage impulse compressor is similar to that of conventional single-stage compressors.

4. Extrapolation of test results to high-speed conditions indicates that impulse compressors operating with subsonic stators can produce pressure rises per stage equal to those now obtainable with conventional axial-flow compressors but with significantly reduced rotational speeds. Some sacrifice in specific quantity flow and perhaps in efficiency, however, would be incurred.

5. Extrapolation of test results to high-speed conditions indicates that impulse compressors operating with supersonic stators can produce pressure rises per stage equal to those reported for supersonic axial-flow compressors but with significantly reduced rotational speeds. Some sacrifice in specific quantity flow, however, would result.

6. Impulse-rotor efficiencies are shown to be very high; hence, there exists the possibility of achieving very high stage efficiency by the application of boundary-layer control to the stationary blades and casings, in which most of the losses occurred.

Langley Aeronautical Laboratory
National Advisory Committee for Aeronautics
Langley Air Force Base, Va., August 10, 1949

APPENDIX

CALCULATION PROCEDURES AND CORRECTION

The more specific explanations and equations used in computing the performance from test data are presented; the more common equations and conversion systems that were used to get test data into basic units are omitted. Each equation origin or justification is also given. All performance parameters are given relative to an intake pressure of 2116 pounds per square foot and 519° F absolute.

The density at entrance to the rotor was found by using the equation

$$\rho_x = \rho_c \left[1 - \left(\frac{p_{s_x} - p_{s_c}}{\gamma p_{s_c}} \right) \left(\frac{p_{s_x} - p_{s_c}}{\frac{2\gamma p_{s_c}}{\gamma - 1}} - 1 \right) \right]$$

This equation consists of the first three terms of a series expansion which converges rapidly in the range of p_{s_x}/p_{s_c} near 1, experienced in these low-speed tests. The relation expanded is

$$\rho_x = \rho_c \left(\frac{p_{s_x}}{p_{s_c}} \right)^{1/\gamma}$$

No change in density is assumed to take place through the rotor.

The power input is calculated from the rate of momentum change across the rotor, or

$$I_2 - I_1 = \int_{r_h^2}^{r_t^2} \left(\rho_2 V_{a_2} V_{tan_2} - \rho_1 V_{a_1} V_{tan_1} \right) 2\pi^2 nr \, d(r^2)$$

The amount of power input that is realized as total-pressure increase in the air is determined by comparing results obtained from flow measurements taken at the positions surveyed. The difference of each point from chamber pressure is used for comparison, that is,

$$E_x = \pi \int_{r_h^2}^{r_t^2} V_{a_x} \left(p_{t_x} - p_{t_c} \right) d(r^2)$$

This equation is an approximation, but for the low values of p_{t_3}/p_{t_1} obtained in these low-speed tests, it yields nearly exact results.

The mass flow measured at each point is

$$m_x = \pi \int_{r_h^2}^{r_t^2} \rho_x V_{a_x} \, d(r^2)$$

The rotor and stage efficiencies would ordinarily be found by the following equations if the calculated mass flows were found to be equal at all positions:

$$\eta_r = \frac{E_2 - E_1}{I_2 - I_1}$$

and

$$\eta_s = \frac{E_3 - E_1}{I_2 - I_1}$$

The mass flows varied as much as 5 percent, however, (fig. 26) so that mass-flow corrections were required. The measured flow at position 2 behind the rotor was used as the correct value for several reasons: first, because it accepts a somewhat more representative sample of the flow and was found to yield most consistent results; second, flows measured at the other two stations were in closer

agreement to flows measured at this station than to each other; third, this system did not result in any impossible rotor efficiencies, and all points fell near a smooth curve.

Two systems of applying the mass-flow correction were tried. The first system made use of the assumption that the total-pressure readings were in error because of turbulence or some other effect. This system yielded poor results: scattered points and impossible rotor efficiencies. Another correction system was therefore used which assumed that the p_s readings were in error. This assumption is probably more logical, because all instruments required p_s correction factors and the instrument itself may set up various pressure fields which depend upon its location, relative size, and the flow conditions. The corrections intended for each static pressure were those which would result in making the mass flows of stations 1 and 3 exactly equal to the station 2 value. The process involves starting with the station 1 or 3 mass flows as known, using the station 2 value, calculating the static pressures which correspond, and then using these new static pressures to calculate the efficiencies. Because the static-pressure affects both the mass-flow and efficiency results in the same way, the intermediate steps can be omitted and the mass-flow ratio applied directly to the energy values for the final result. The similarity of the equations for calculating the mass flow m and power available E are indicated by the following:

$$m_x = \pi \int_{r_h^2}^{r_t^2} \rho_x V_{a_x} \, d(r^2)$$

$$= \int_{r_h^2}^{r_t^2} \rho_x \cos \phi_x \sqrt{\frac{2}{\rho_x}\left(p_{t_x} - p_{s_x}\right)} \, d(r^2)$$

$$E_x = \pi \int_{r_h^2}^{r_t^2} V_{a_x}\left(p_{t_x} - p_{t_c}\right) d(r^2)$$

$$= \pi \int_{r_h^2}^{r_t^2} \left[\cos \phi_x \sqrt{\frac{2}{\rho_x}\left(p_{t_x} - p_{s_x}\right)}\right]\left(p_{t_x} - p_{t_c}\right) d(r^2)$$

The power input has the static-pressure factor appearing twice. Thus,

$$I_x = 2\pi^2 n \int_{r_h^2}^{r_t^2} \rho_x V_{a_x} V_{\tan x} r \, d(r^2)$$

$$= 2\pi^2 n \int_{r_h^2}^{r_t^2} \rho_x \left[\cos \phi_x \sqrt{\frac{2}{\rho_x}\left(p_{t_x} - p_{s_x}\right)}\right]\left[\sin \phi_x \sqrt{\frac{2}{\rho_x}\left(p_{t_x} - p_{s_x}\right)}\right] r \, d(r^2)$$

Consequently, the mass ratio must appear twice in the correction.

The effect of the small static-pressure correction on the density has been found to be negligible, and is therefore omitted. The following equations were therefore used for the efficiency curves presented:

$$\eta_r = \frac{E_2 - E_1 \frac{m_2}{m_1}}{I_2 - I_1 \left(\frac{m_2}{m_1}\right)^2}$$

and

$$\eta_s = \frac{E_2 \frac{m_2}{m_3} - E_1 \frac{m_2}{m_1}}{I_2 - I_1 \left(\frac{m_2}{m_1}\right)^2}$$

The calculations for the theoretical values presented as comparisons with test results are the usual incompressible, isentropic relations used with low-speed flow. Turning-angle values from two-dimensional cascade tests were used.

REFERENCES

1. Sinnette, John T., Jr., Schey, Oscar W., and King, J. Austin: Performance of NACA Eight-Stage Axial-Flow Compressor Designed on the Basis of Airfoil Theory. NACA Rep. 758, 1943.

2. Sörensen, E.: Constant-Pressure Blowers. NACA TM 927, 1940.

3. Weise, A.: Supersonic Axial Compressor. British Ministry of Supply TPA3/TIB Translation No. GDC 10/6116 T, Oct. 1943.

4. Perl, W., and Tucker, M.: A General Representation for Axial-Flow Fans and Turbines. NACA Rep. 814, 1945.

5. Bogdonoff, Seymour M., and Bogdonoff, Harriet E.: Blade Design Data for Axial-Flow Fans and Compressors. NACA ACR L5F07a, 1945.

6. Bogdonoff, Seymour M., and Herrig, L. Joseph: Performance of Axial-Flow Fans and Compressor Blades Designed for High Loadings. NACA TN 1201, 1947.

7. Schwartz, Ira R.: Investigations of an Annular Diffuser-Fan Combination Handling Rotating Flow. NACA RM L9B28, 1949.

8. Bogdonoff, Seymour M.: N.A.C.A. Cascade Data for the Blade Design of High-Performance Axial-Flow Compressors. Jour. Aero. Sci., vol. 15, no. 2, Feb. 1948, pp. 89-95.

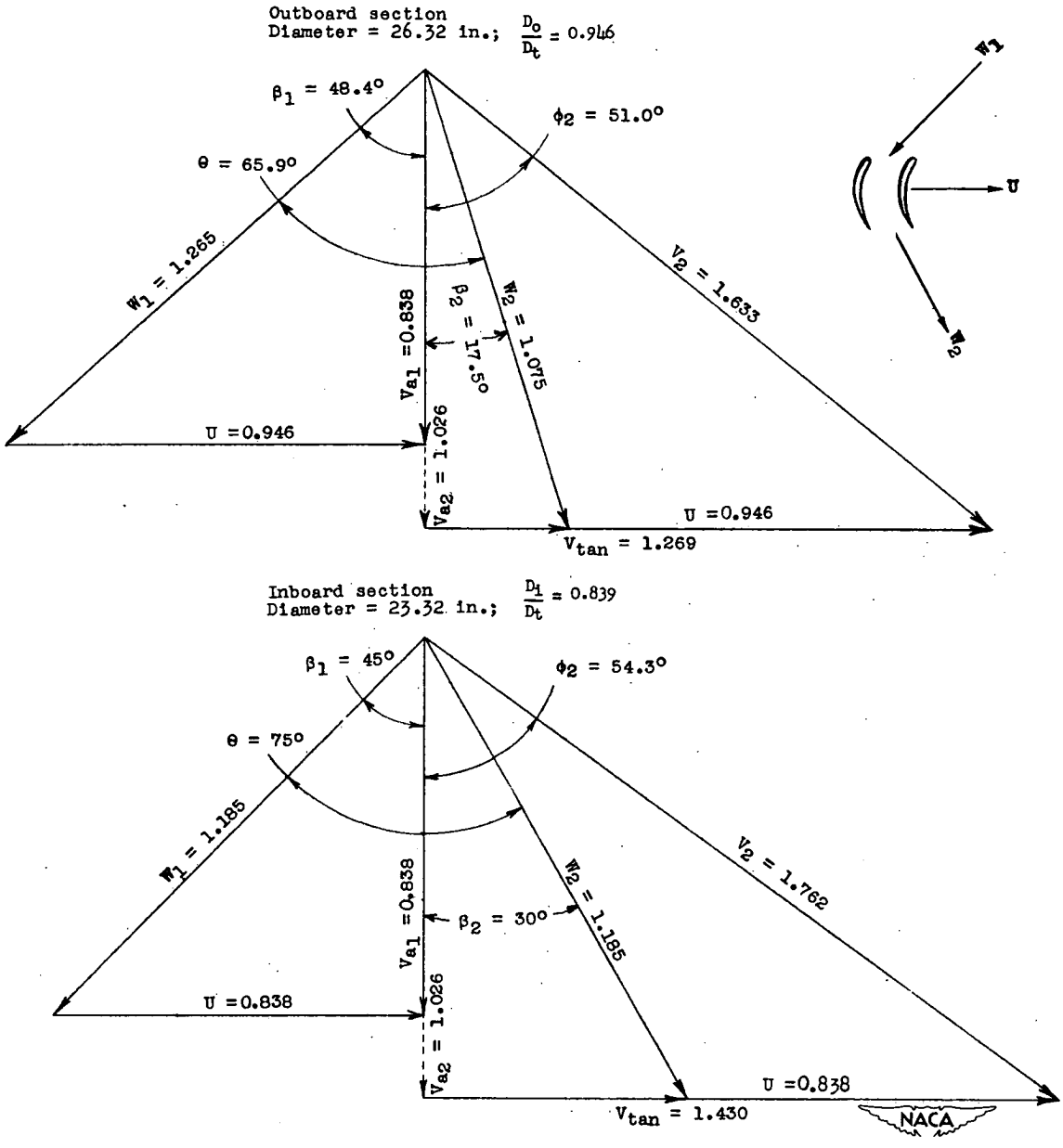

Figure 1.— Expected velocity diagrams for impulse rotor, given as a ratio of U_t = 145.66 feet per second.

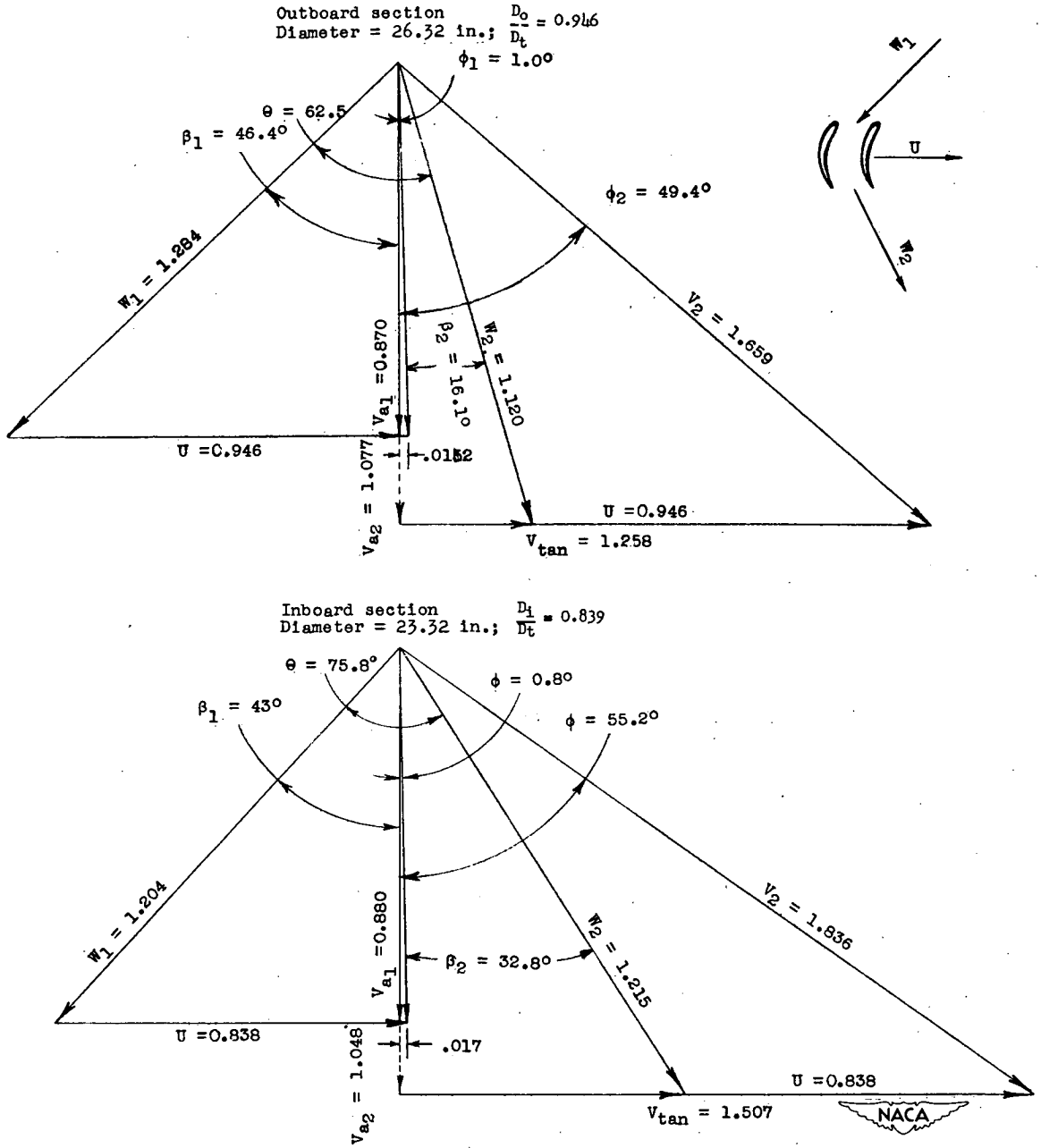

Figure 2.- Experimental velocity diagrams for impulse rotor, given as a ratio of U_t = 145.66 feet per second.

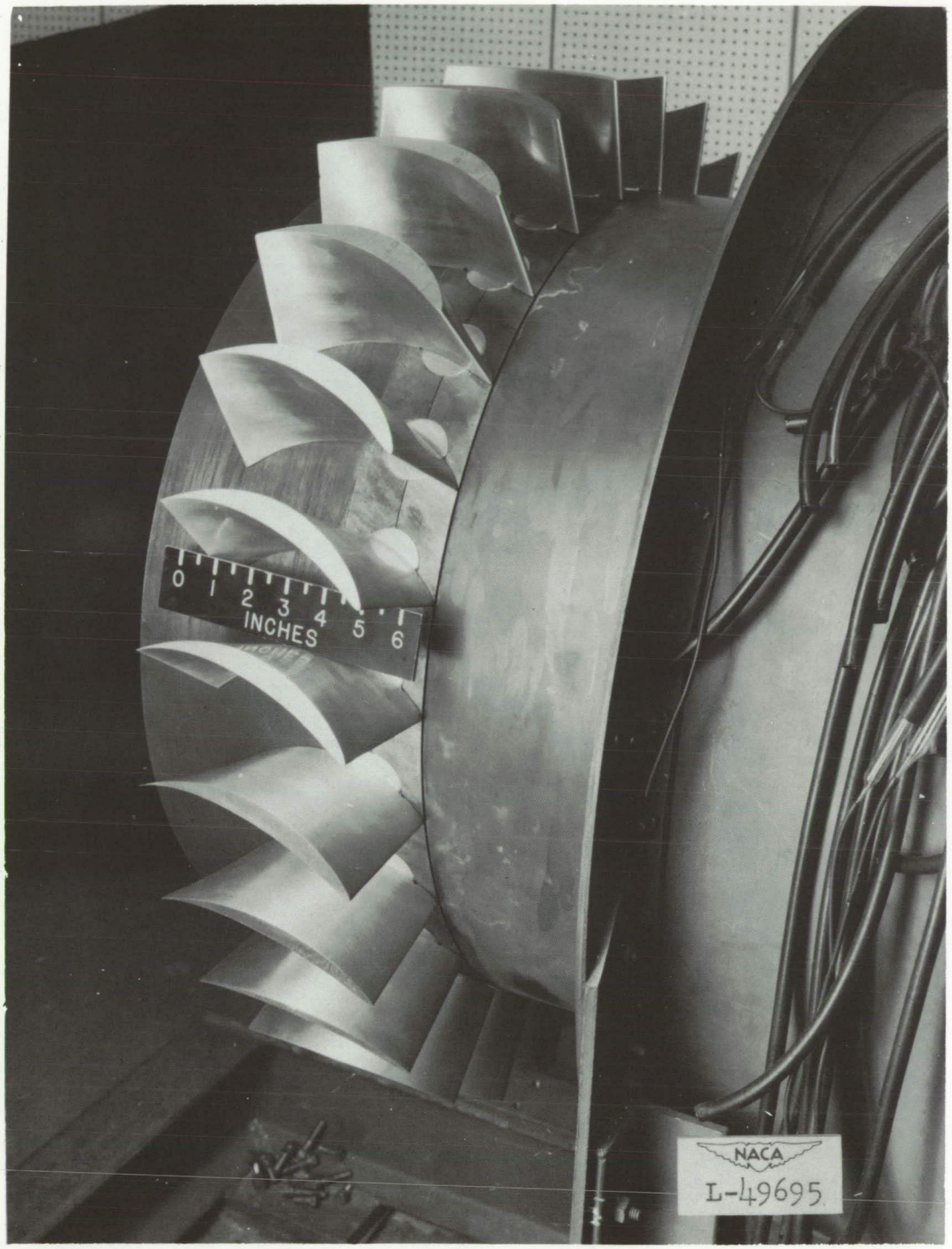

Figure 3.- Rotor assembly before area change was added.

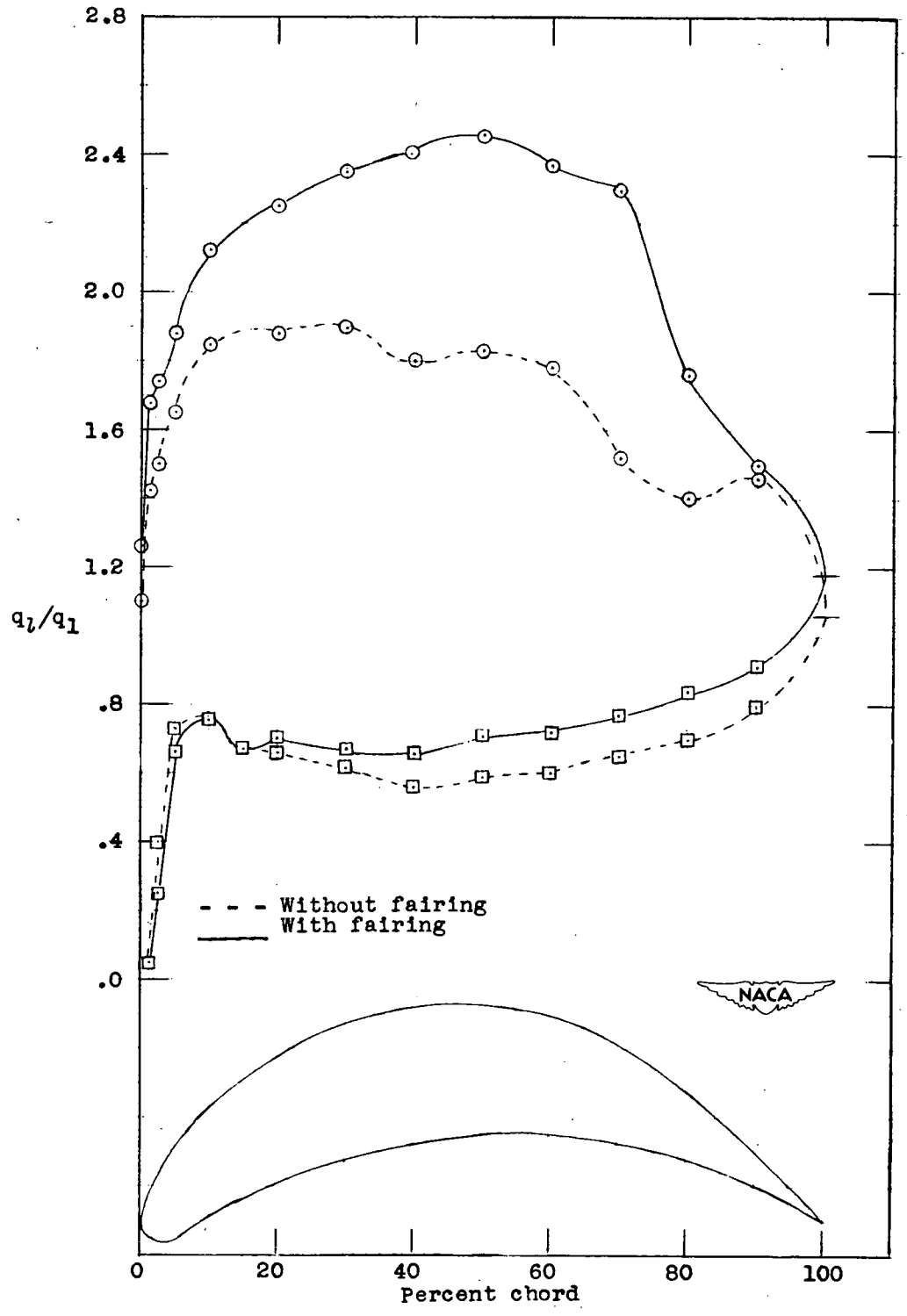

Figure 4.– Pressure distribution of blade 1 in cascade. Circular-arc mean line and constant passage area. $\alpha = 40^\circ$; $\theta = 75^\circ$; $\beta = 45^\circ$; $\sigma = 2.0$.

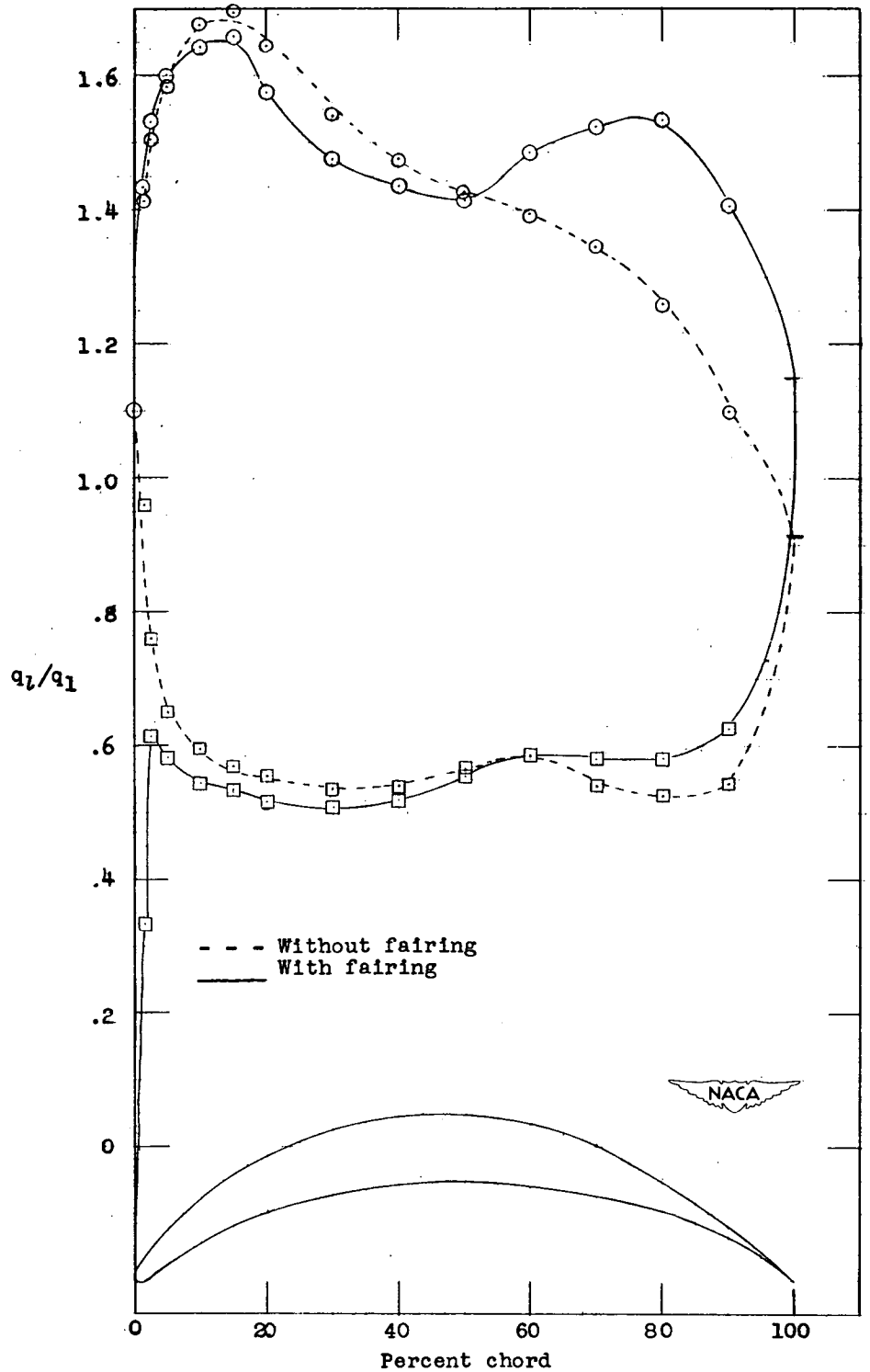

Figure 5.– Pressure distribution of blade 2 in cascade. Circular-arc mean line with NACA 65-010 thickness distribution. $\alpha = 44.5^\circ$; $\theta = 76.8^\circ$; $\beta = 45^\circ$; $\sigma = 2.0$.

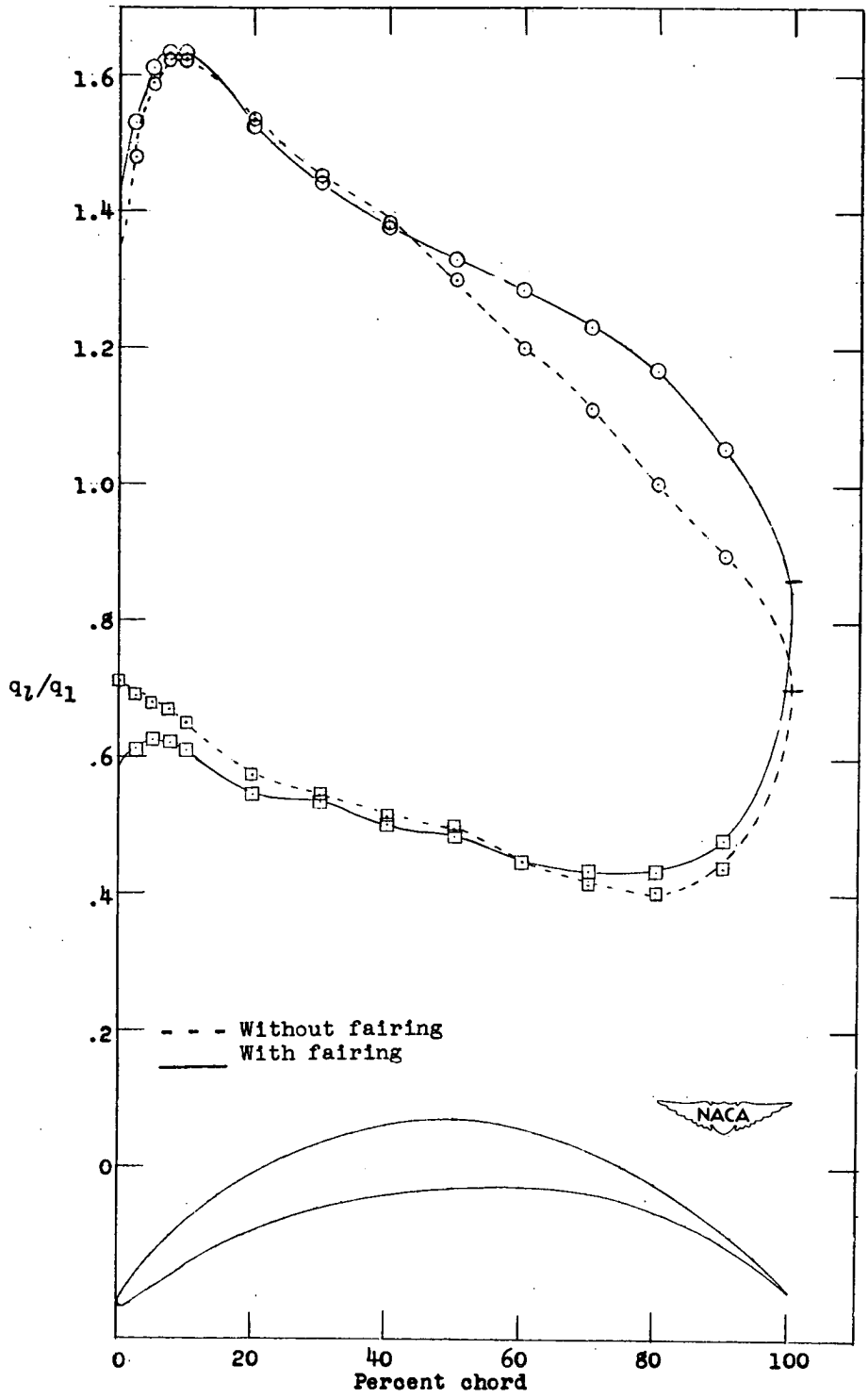

Figure 6.— Pressure distribution of blade 3 in cascade. Circular-arc mean line with NACA 65-010 thickness distribution. $\alpha = 43^\circ$; $\theta = 75^\circ$; $\beta = 45^\circ$; $\sigma = 2.0$.

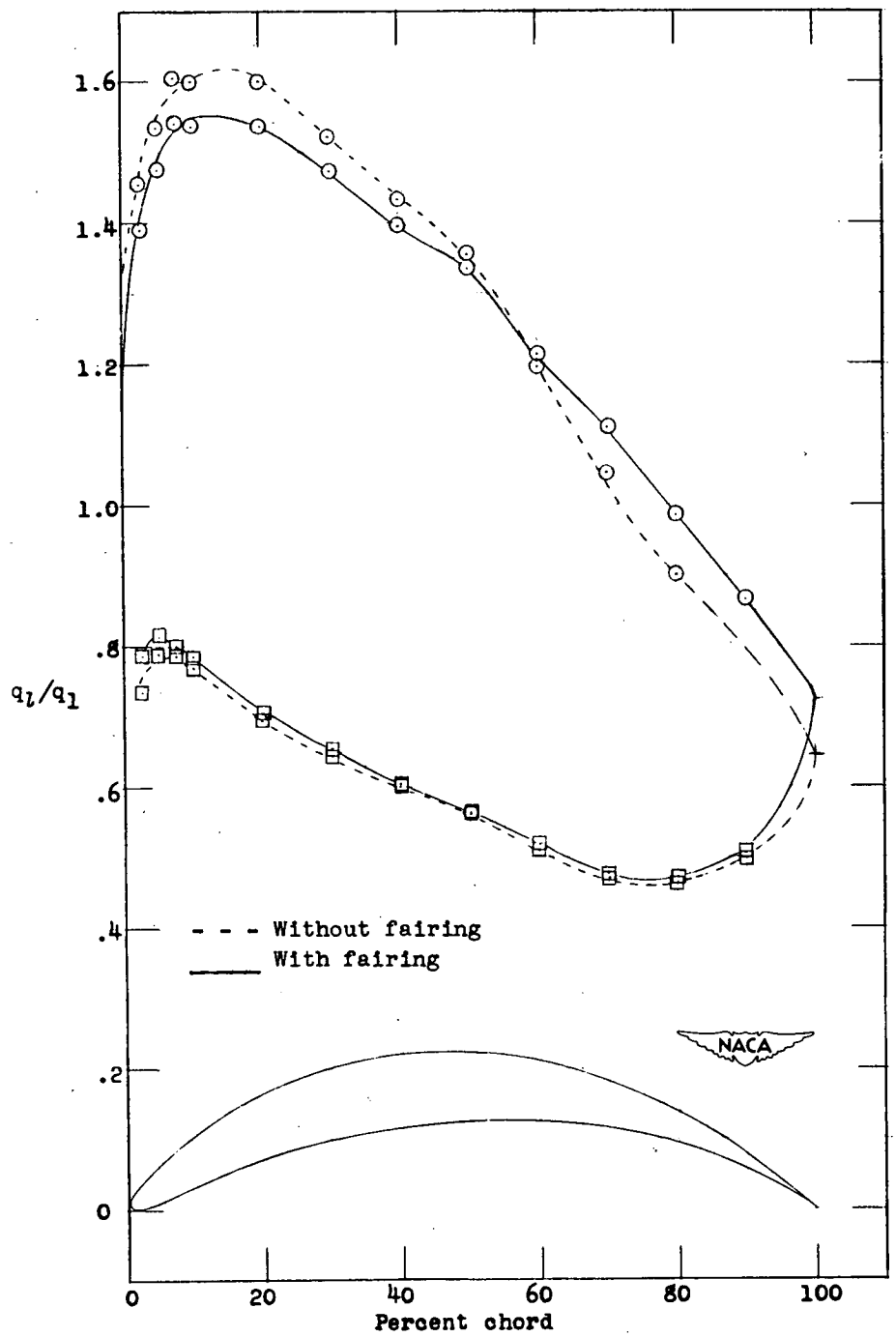

Figure 7.– Pressure distribution of blade 4 in cascade. Circular-arc mean line with NACA 65-010 thickness distribution. $\alpha = 37.8^\circ$; $\theta = 65^\circ$; $\beta = 48.5^\circ$; $\sigma = 2.0$.

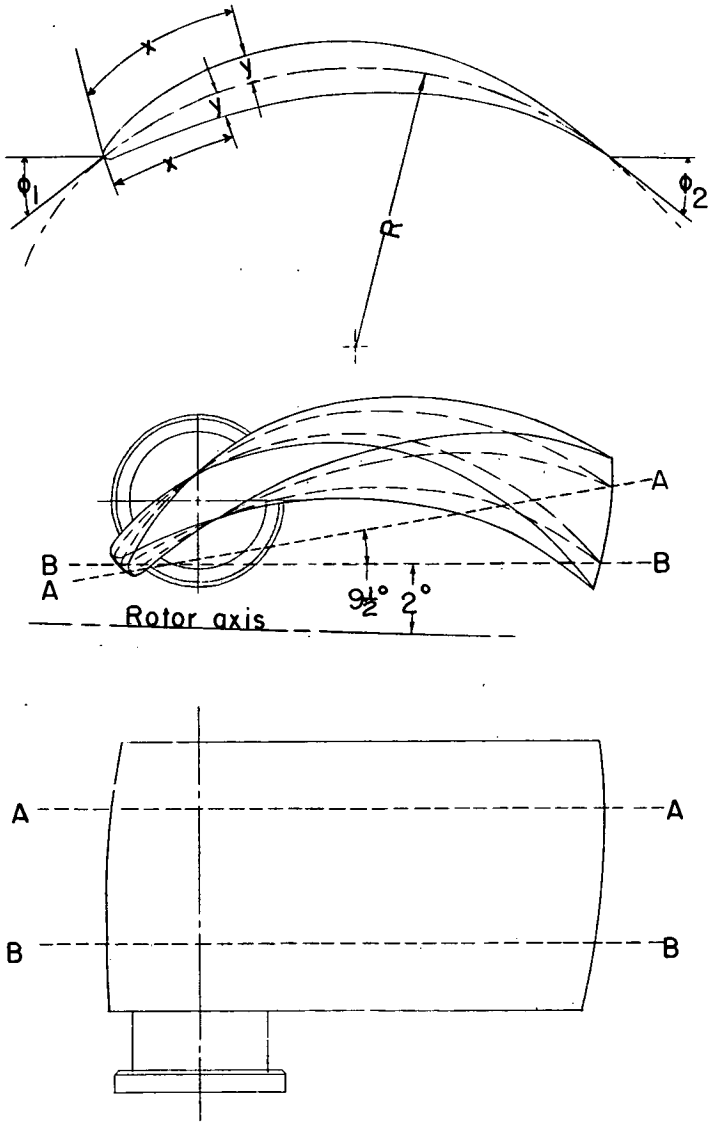

Airfoil Coordinates

x	y
0.030	0.045
.045	.053
.075	.067
.150	.094
.300	.133
.450	.163
.600	.187
.900	.225
1.200	.253
1.500	.274
1.800	.289
2.100	.299
2.400	.303
2.700	.302
3.000	.292
3.300	.274
3.600	.249
3.900	.218
4.200	.182
4.500	.147
4.800	.111
5.100	.075
5.400	.045
5.700	.021
6.000	.009
A–A: R = 4.245	
B–B: R = 3.799	
L. E. radius: 0.040	

NACA

Figure 8.– Sketch and coordinates of impulse rotor blade.

Figure 9.- Photograph of rotor blade.

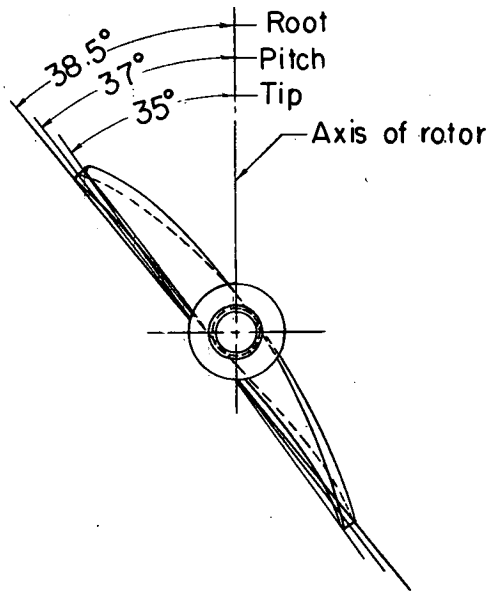

Airfoil Coordinates

x_U	y_U	x_L	y_L
0	0	0	0
.017	.055	.038	−.017
.037	.076	.051	−.017
.089	.117	.076	−.018
.198	.182	.136	−.017
.309	.233	.252	−.011
.421	.277	.366	−.004
.647	.348	.479	.003
.876	.403	.703	.015
1.104	.446	.925	.027
1.332	.479	1.146	.037
1.562	.502	1.368	.046
1.791	.517	1.588	.054
2.021	.522	1.809	.062
2.250	.517	2.029	.069
2.479	.501	2.250	.079
2.707	.476	2.471	.090
2.935	.441	2.693	.103
3.161	.399	2.915	.115
3.387	.351	3.139	.126
3.611	.297	3.363	.132
3.834	.237	3.589	.133
4.057	.173	3.816	.126
4.279	.101	4.043	.107
4.503	.006	4.271	.070
		4.497	−.006
L. E. radius: 0.030			

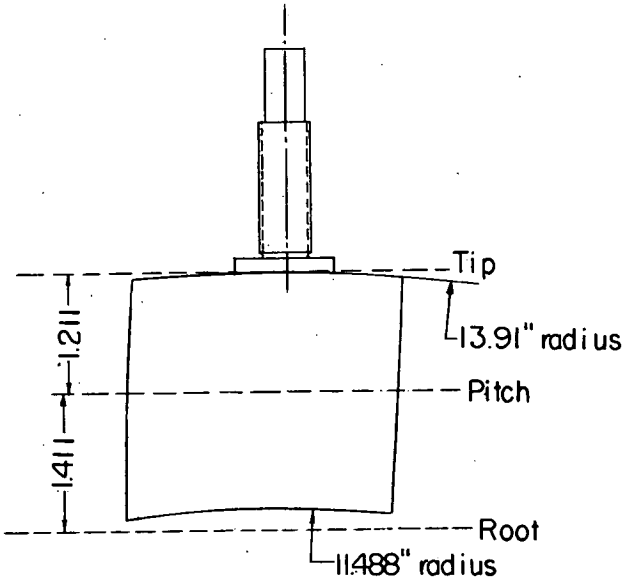

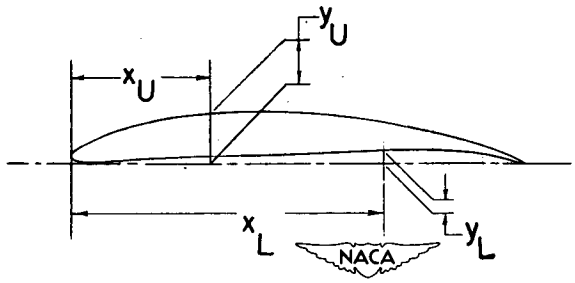

Figure 10.– Sketch and coordinates of NACA 65–(12)10 stator blade.

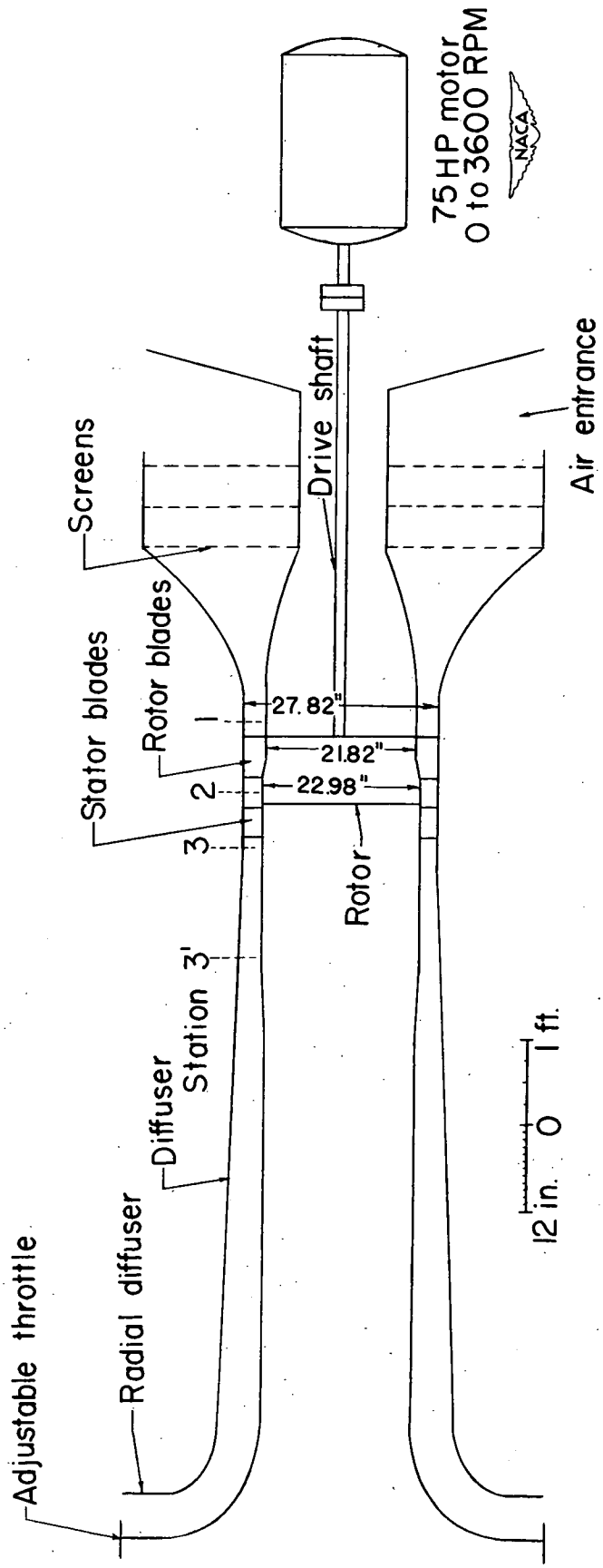

Figure 11.- Schematic diagram of test setup.

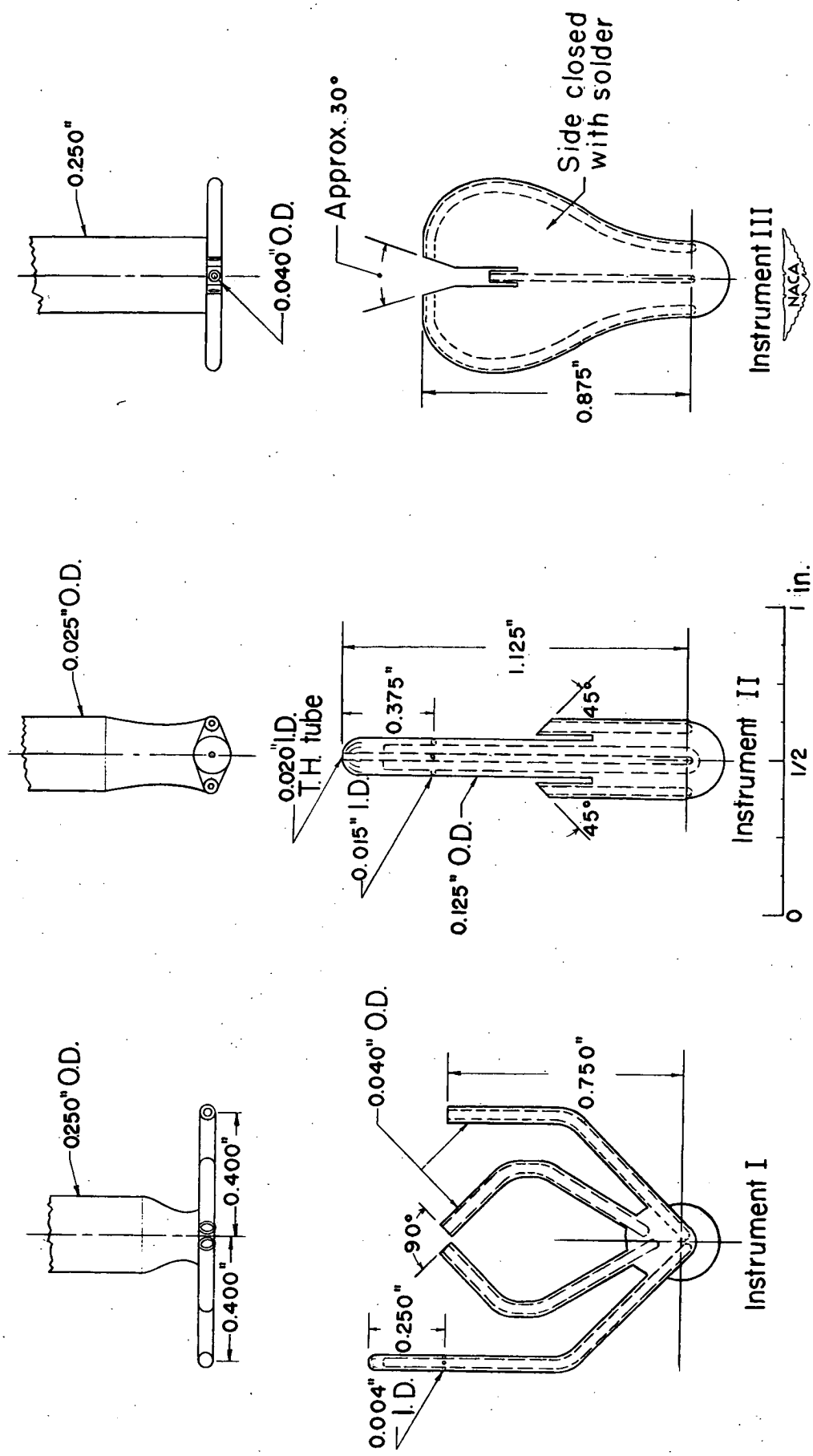

Figure 12.- Sketches of the three survey instruments used with general dimensions.

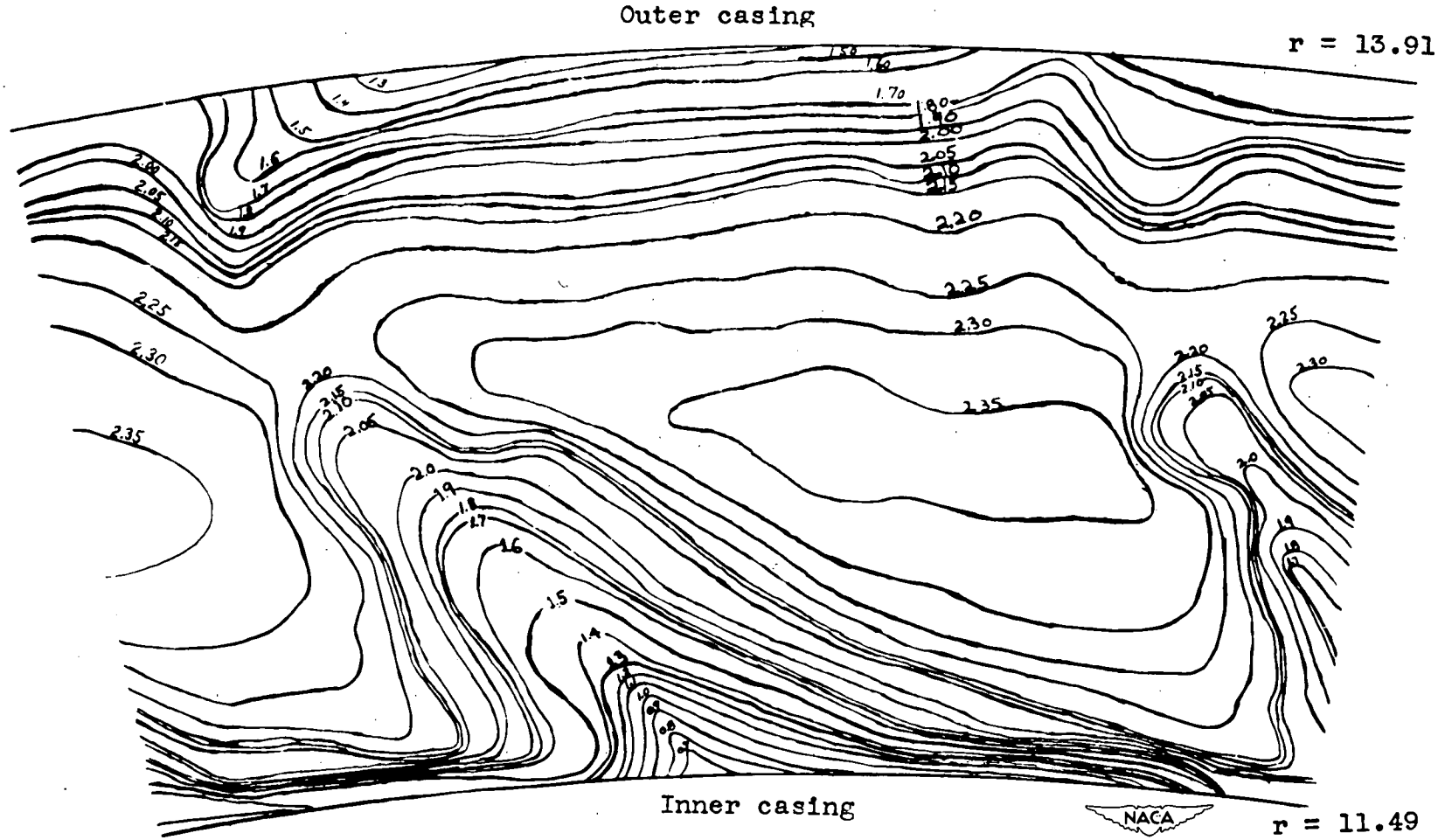

Figure 13.– Graphical representation of the flow field one–half chord length behind the stators. Contours show constant values of total–pressure–rise coefficient, $\frac{\Delta p_t}{\frac{1}{2}\rho U_t^2}$.

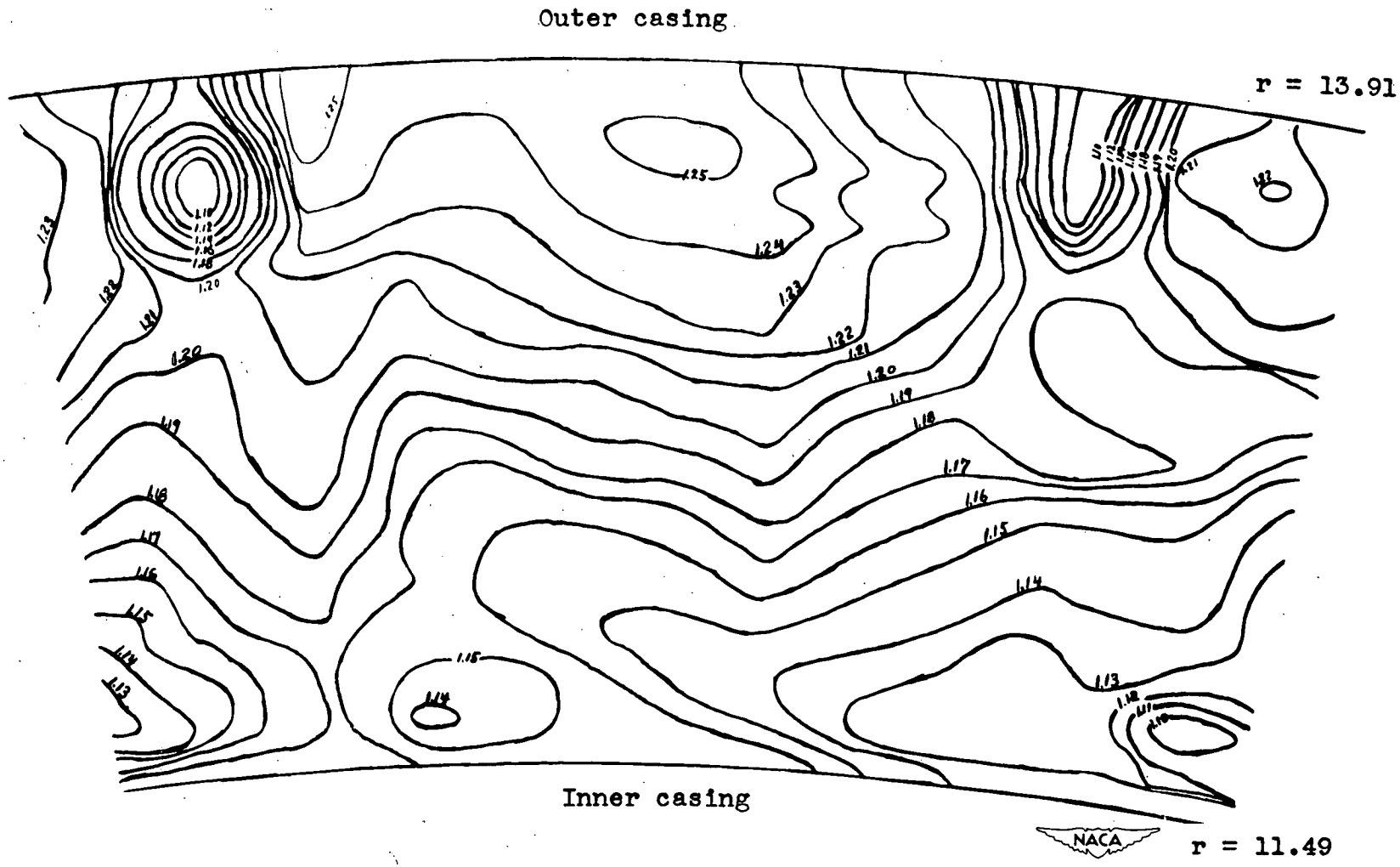

Figure 14.– Graphical representation of the flow field one-half chord length behind the stators. Contours show constant values of static-pressure-rise coefficient, $\frac{\Delta p_s}{\frac{1}{2}\rho U_t^2}$.

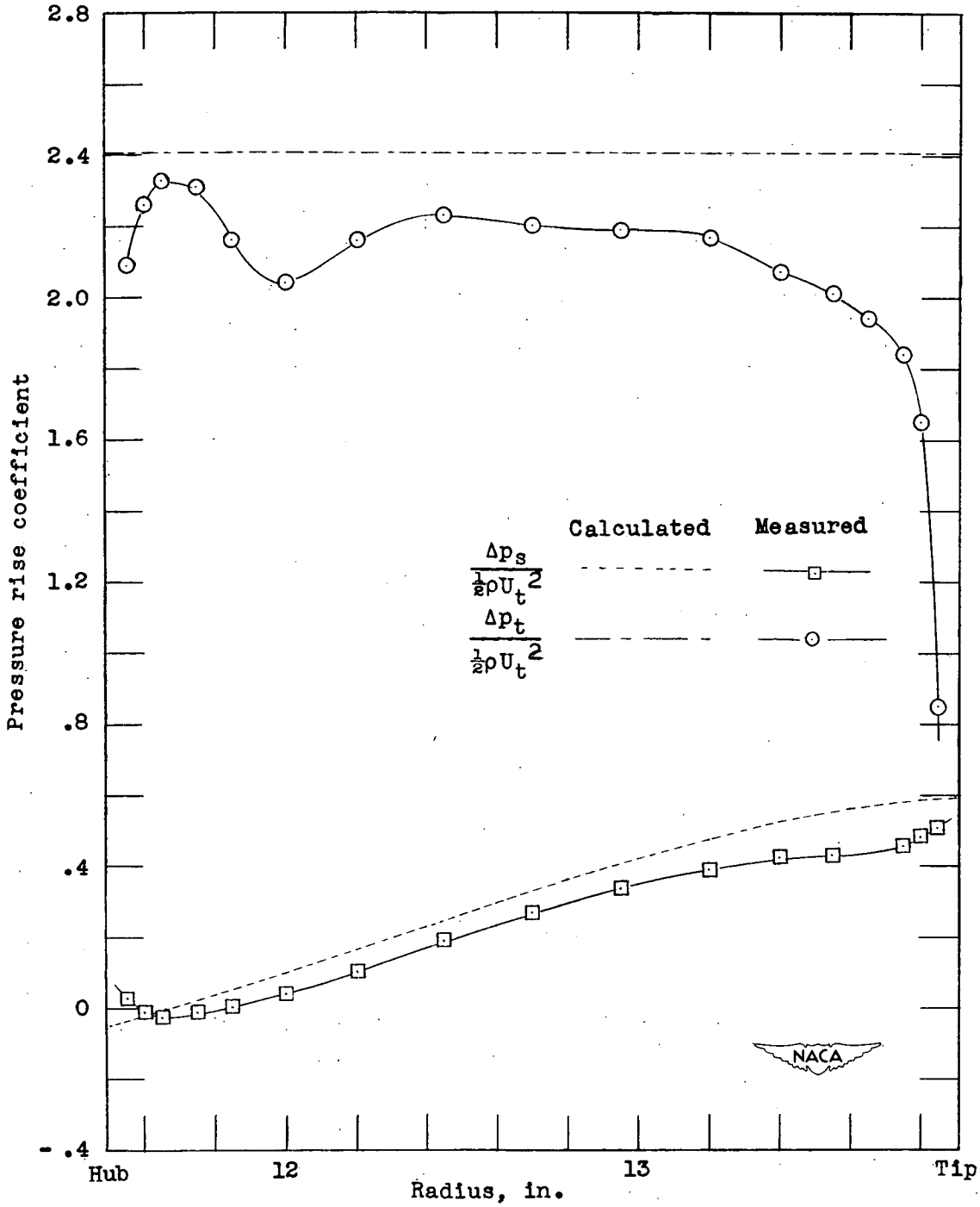

Figure 15.– Variation of total– and static–pressure rise across annulus. Calculated and measured values at design conditions for rotor.

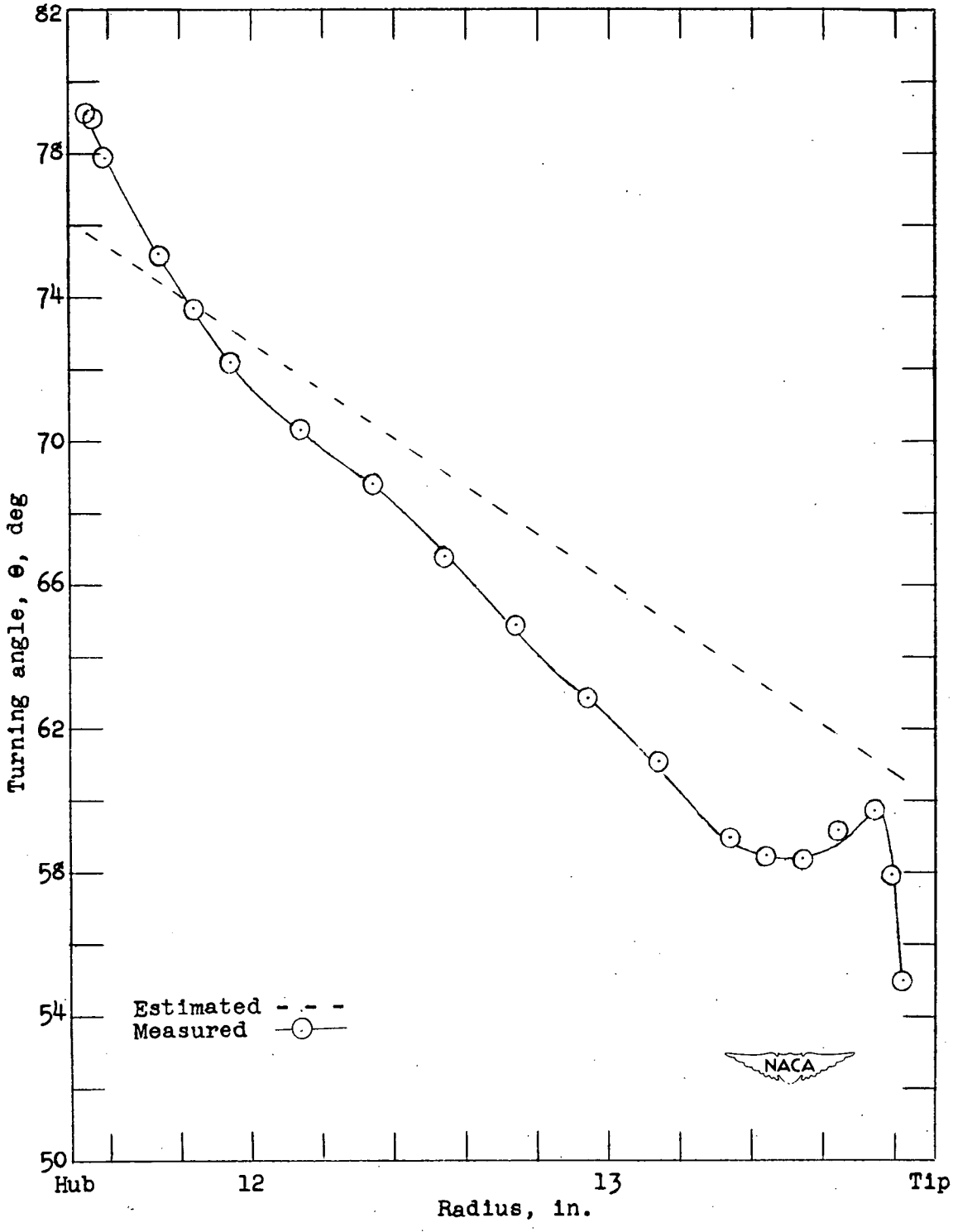

Figure 16.– Estimated and measured turning angle of the air by the rotor from hub to tip at design condition.

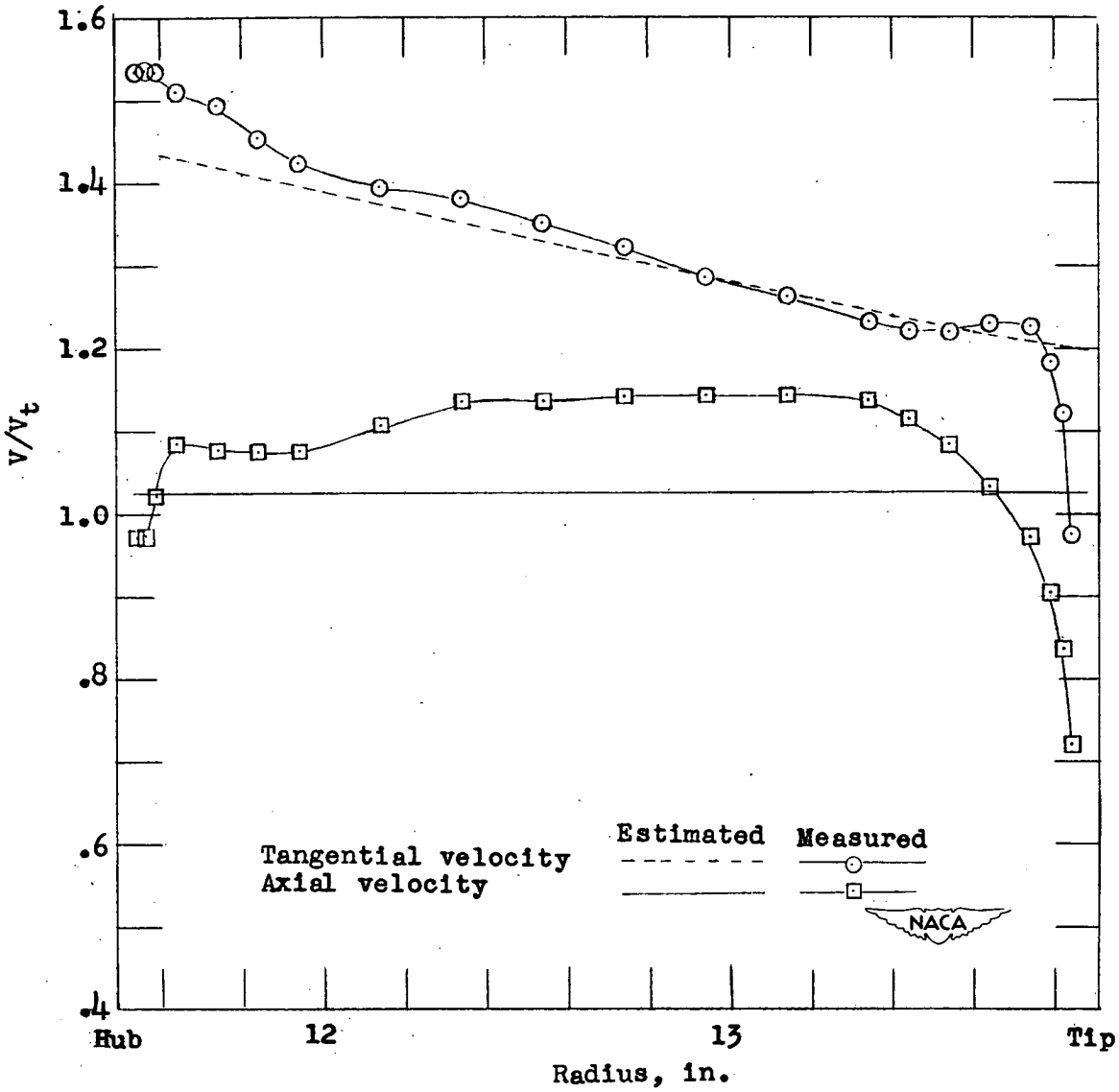

Figure 17.- Axial and tangential velocities from hub to tip. Estimated and measured values behind the rotor at design condition.

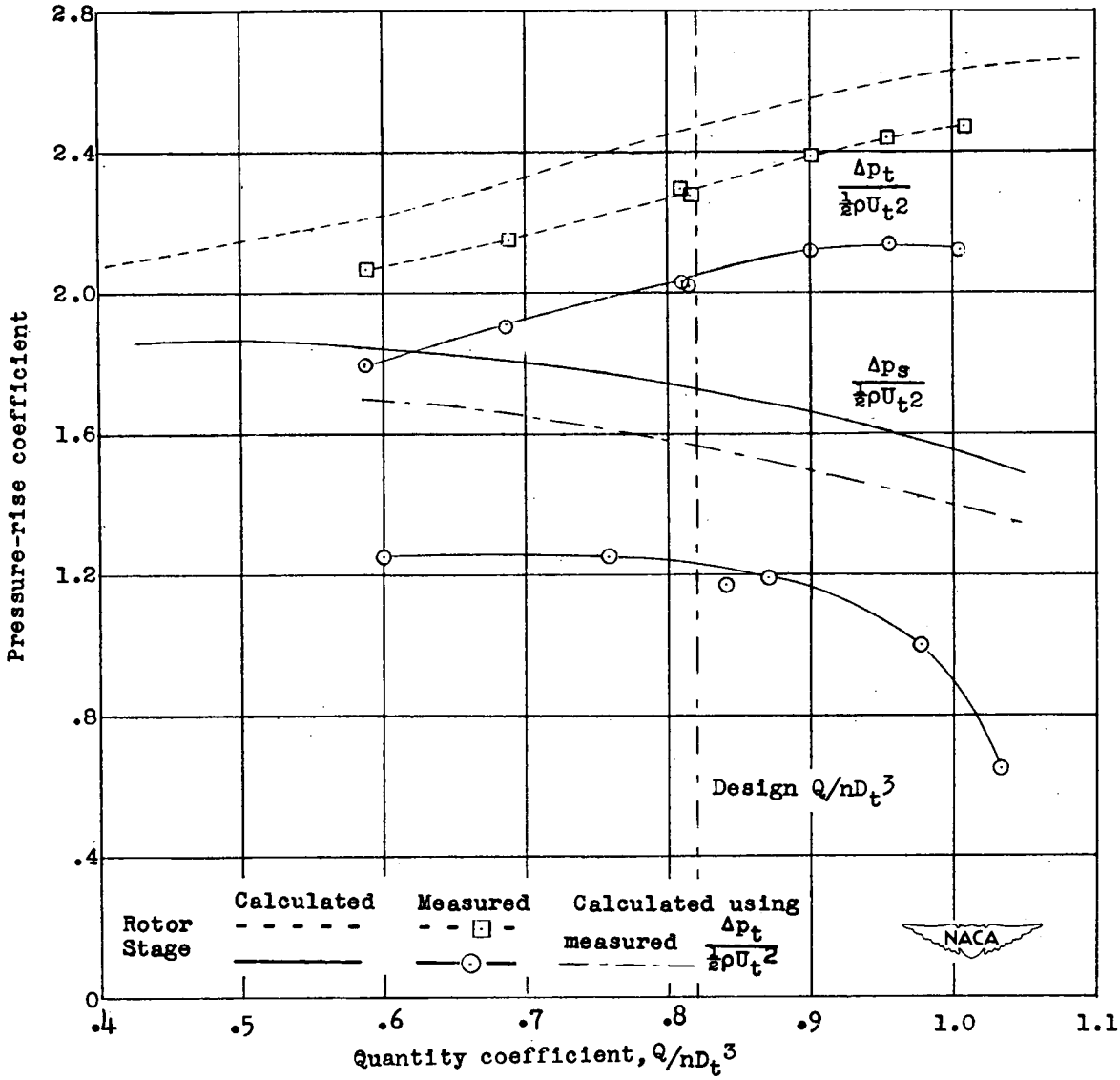

Figure 18.– Variation of weighted average pressure–rise coefficients with quantity coefficient.

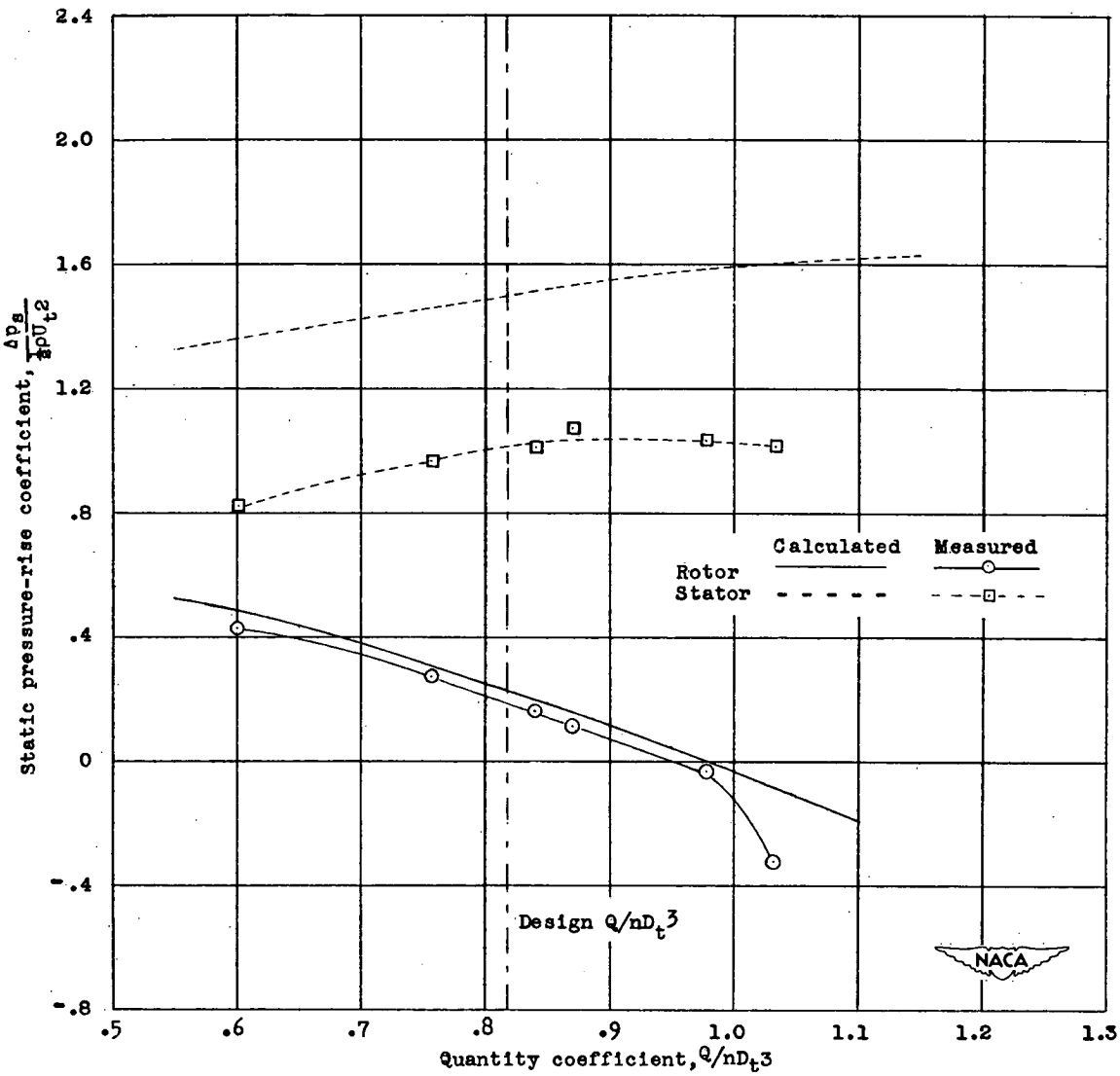

Figure 19.- Variation of weighted average static-pressure-rise coefficients for rotor and stator individually.

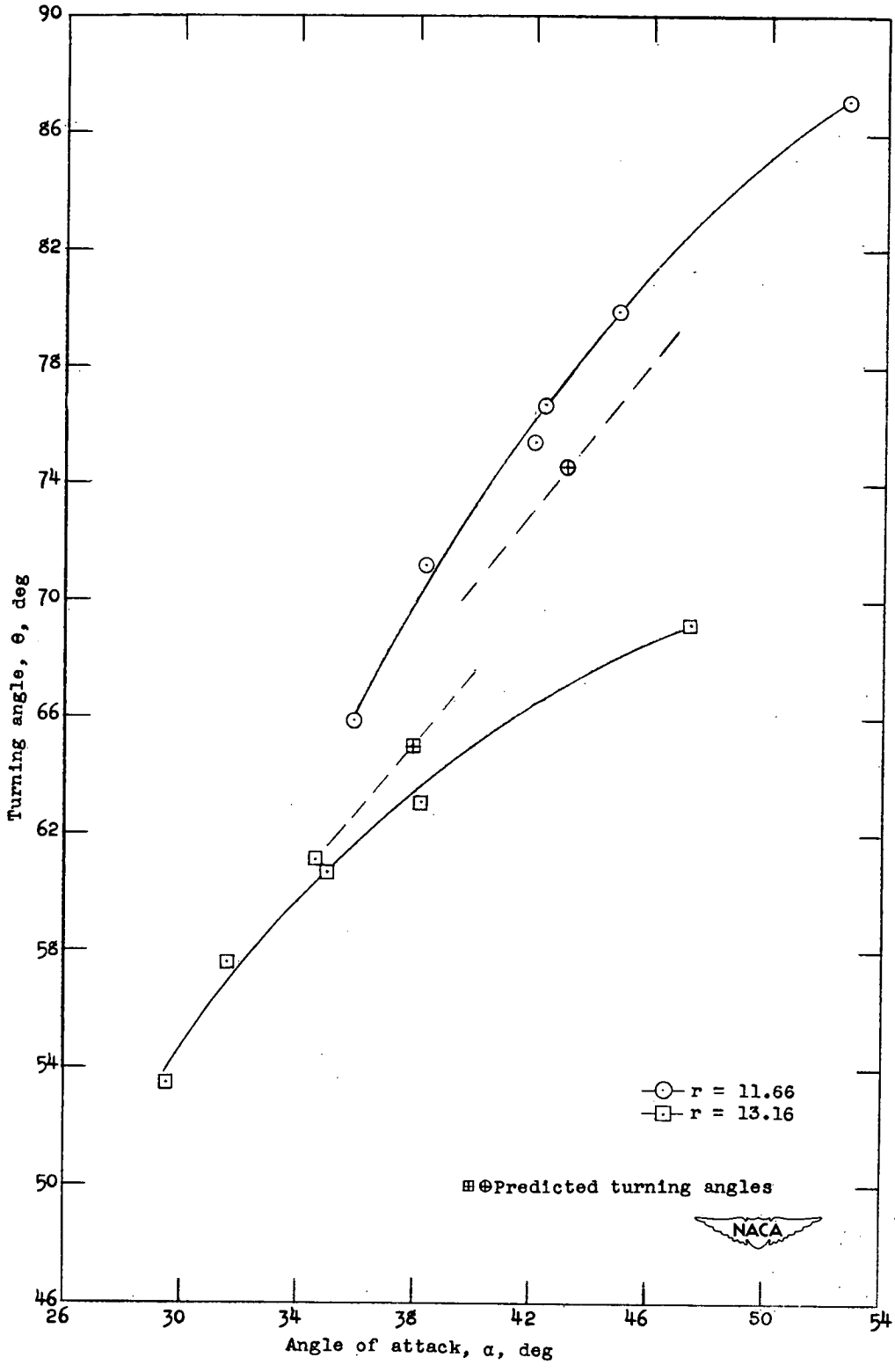

Figure 20.– Variation of turning angle with angle of attack for rotor at the two design radii.

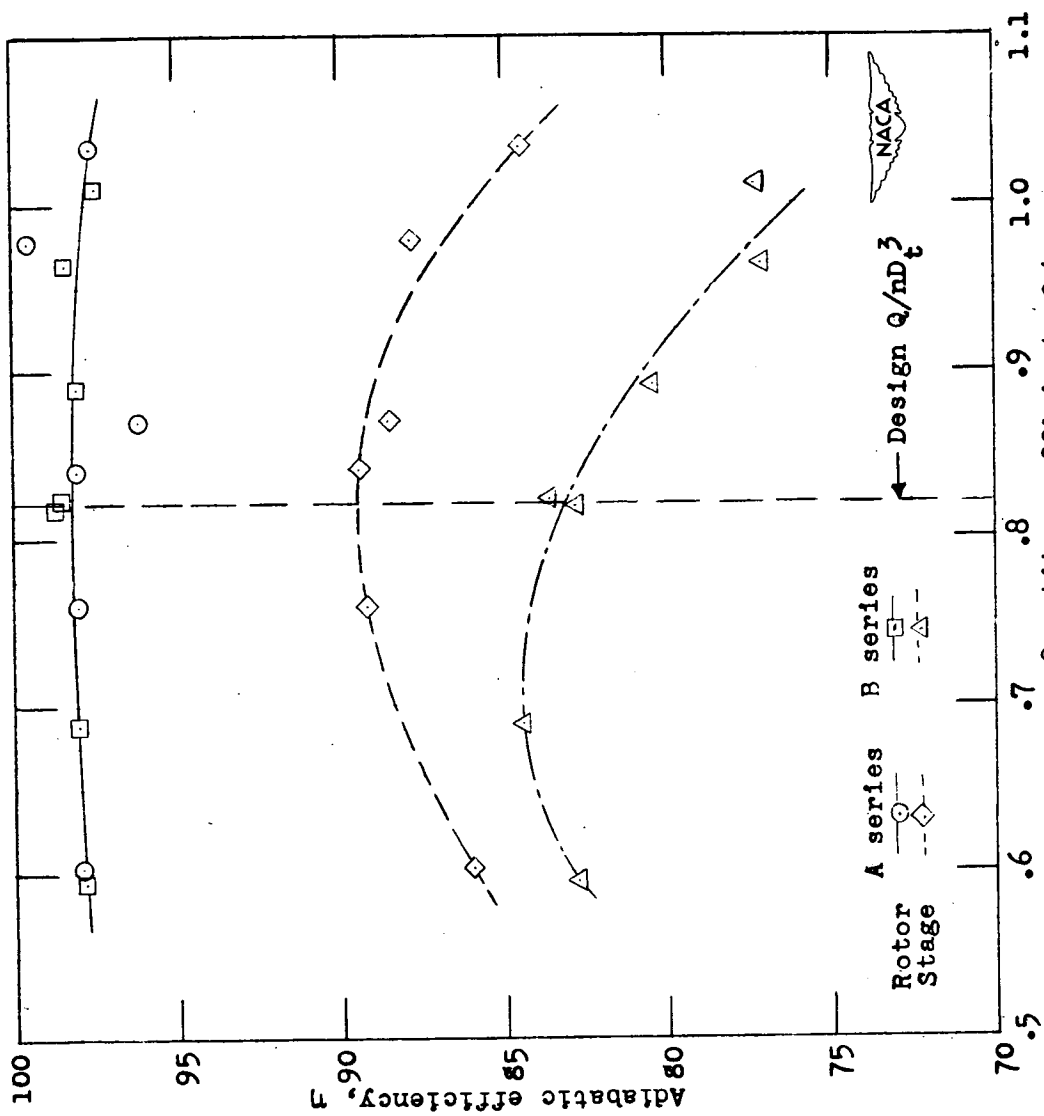

Figure 21.- Variation of efficiency with quantity coefficient for rotor alone and also the entire stage. (Both series of tests are shown.)

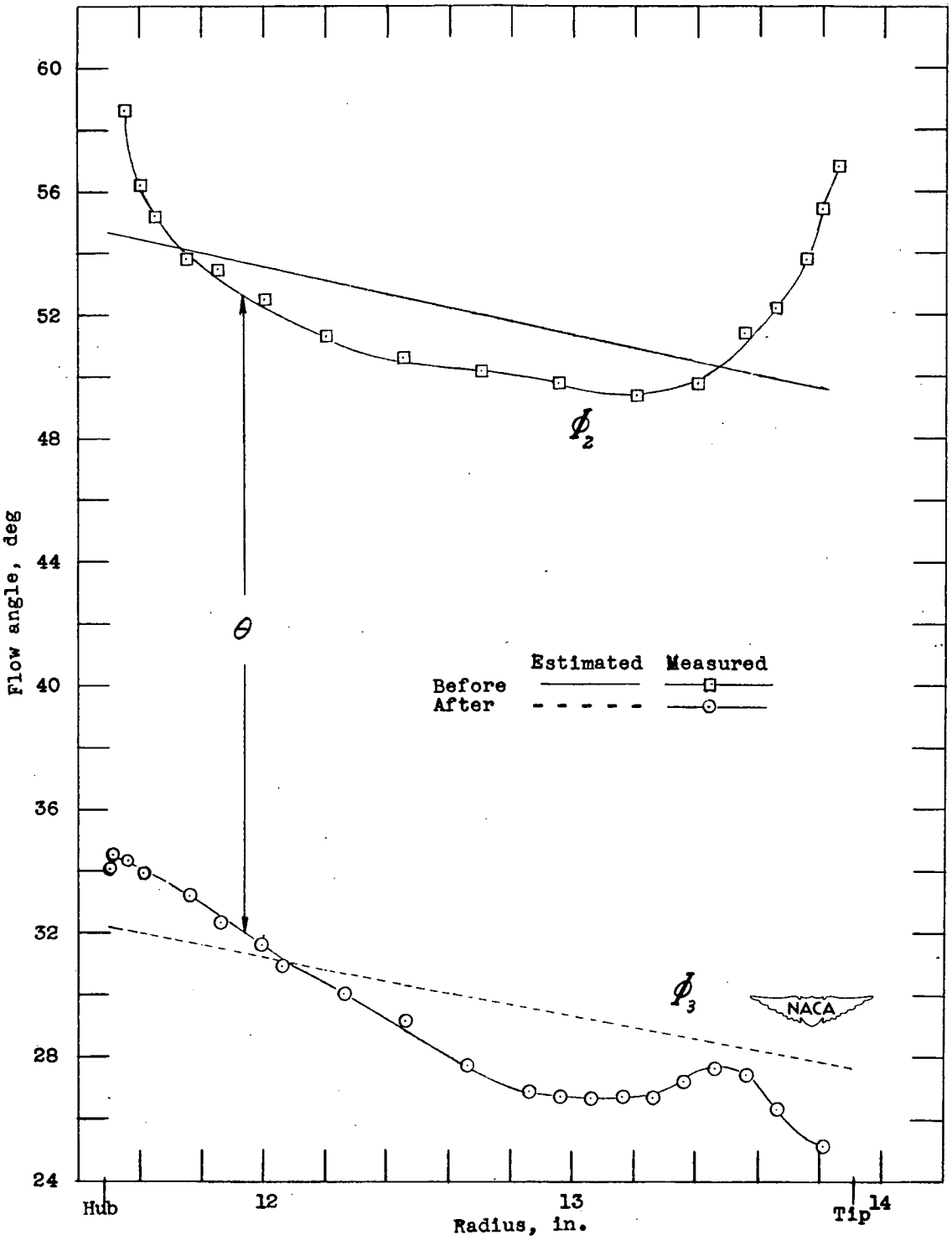

Figure 22.– Radial distribution of the air direction before and after stator. Estimated and measured values at 1200 rpm.

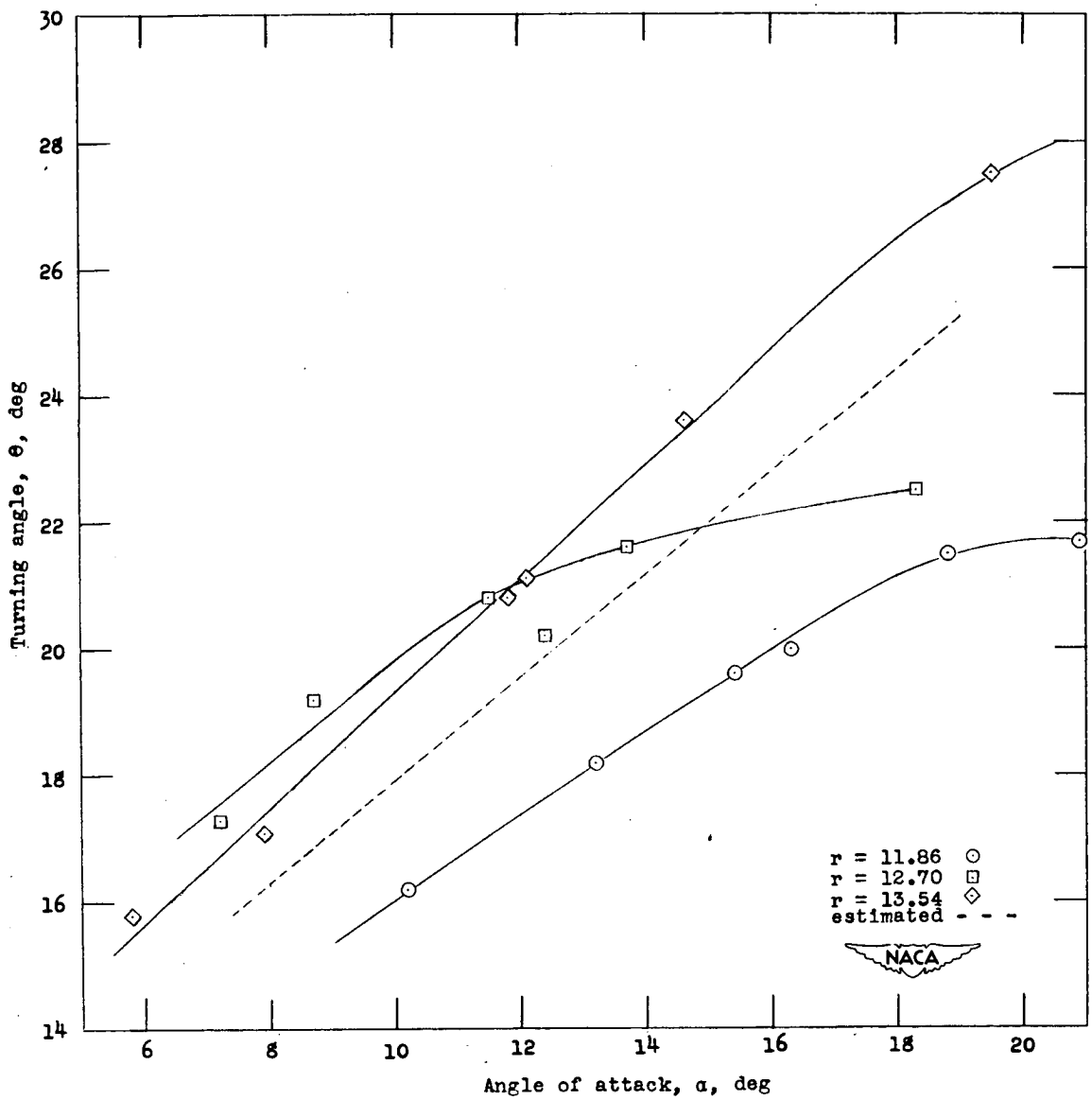

Figure 23.- Variation of turning angle with angle of attack for stator at three radii.

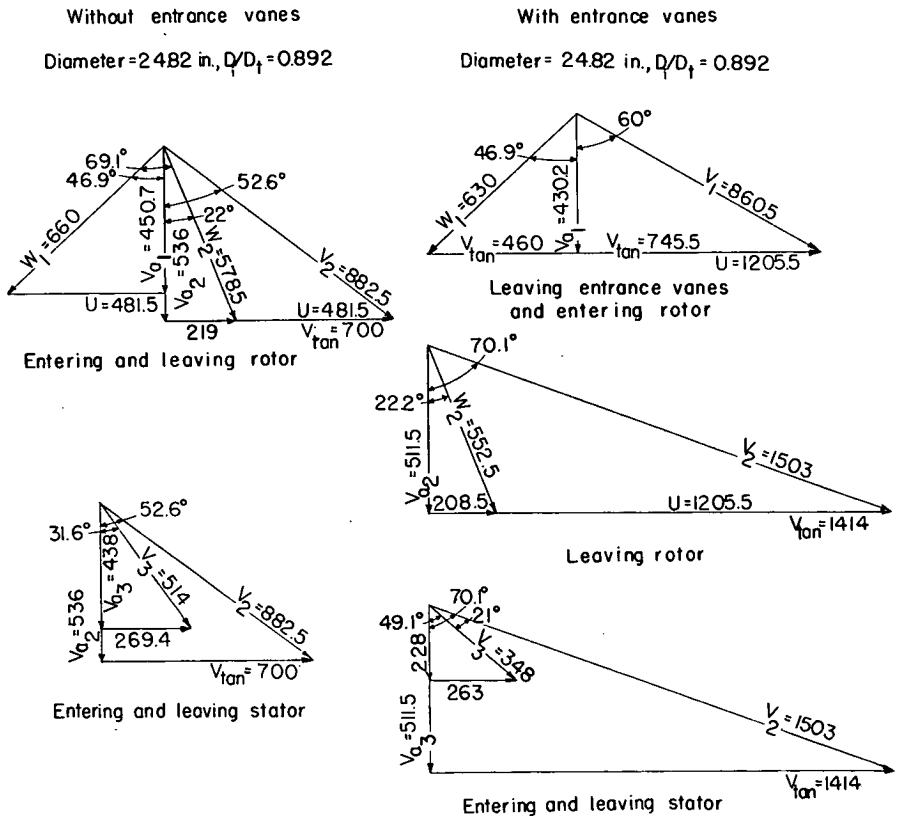

Synopsis of Theoretical Calculations

	Mach number	Velocity (fps)	p_s/p_{t_c}	p_t/p_{t_c}
Without entrance vanes				
Entering annulus	0.410	450.7	0.891	1.000
Entering rotor[1]	.600	660.0	.891	1.137
Leaving rotor[1]	.522	578.5	.938	1.130
Entering stator	.797	882.5	.940	1.429
Leaving stator	.446	514.0	1.221	1.400
With entrance vanes				
Entering vanes	0.296	328.0	0.941	1.000
Leaving vanes	.820	860.5	.643	1.000
Entering rotor[1]	.600	630.0	.643	.820
Leaving rotor[1]	.522	552.5	.664	.800
Entering stator	1.420	1503.0	.667	2.178
Leaving stator	.280	348.0	1.966	2.046

[1]Rotor coordinates.

NACA

Figure 24.– Velocity diagrams and chart of results for theoretical calculations of high-speed operation.

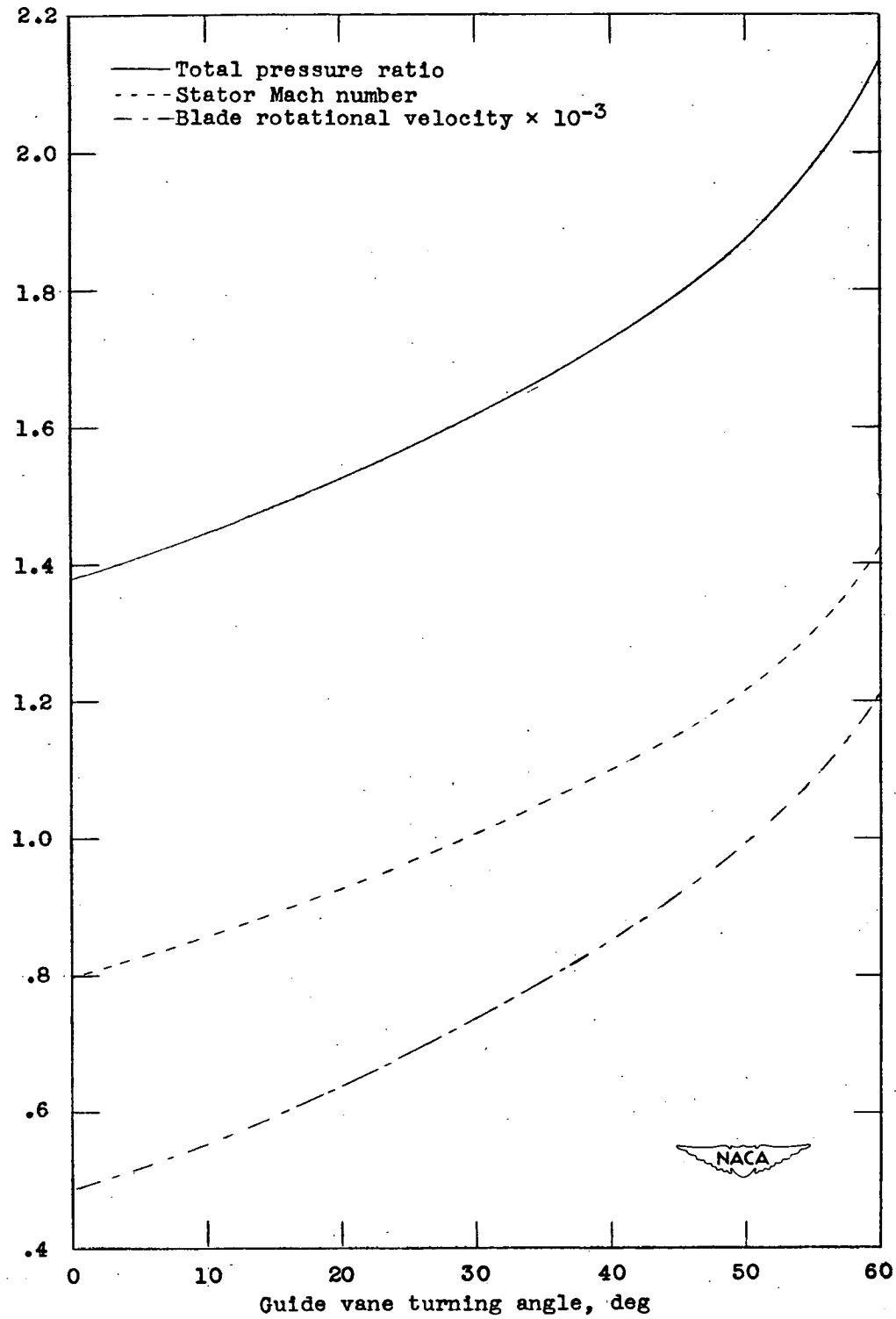

Figure 25.– Extrapolation of low-speed test results to high rotational speed. Measured rotor and stage efficiencies, and a constant rotor blade Mach number of 0.60 were used.

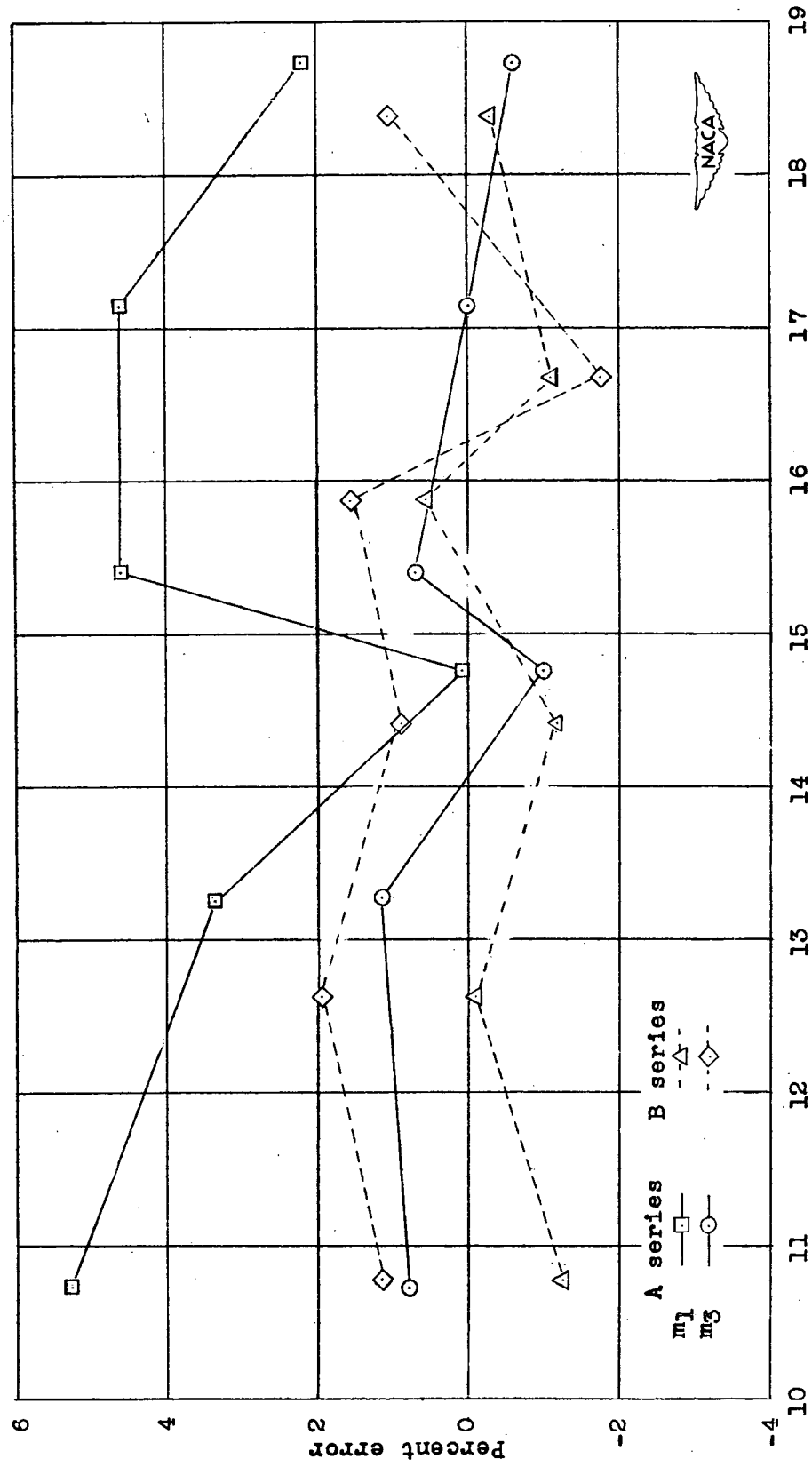

Figure 26.- Differences in measured weight flow of survey stations expressed in percentage of station 2 weight flow.